2006-03

Development and evolution of cirrus in a mesoscale model

Lewis, Michael M.

Monterey, California. Naval Postgraduate School

NAVAL POSTGRADUATE SCHOOL

MONTEREY, CALIFORNIA

THESIS

DEVELOPMENT AND EVOLUTION OF CIRRUS IN A MESOSCALE MODEL

By

Michael Moore Lewis

March 2006

Thesis Advisor:	Wendell A. Nuss
Second Reader:	Phillip A. Durkee

Approved for public release; distribution is unlimited

THIS PAGE INTENTIONALLY LEFT BLANK

REPORT DOCUMENTATION PAGE			Form Approved OMB No. 0704-0188
Public reporting burden for this collection of information is estimated to average 1 hour per response, including the time for reviewing instruction, searching existing data sources, gathering and maintaining the data needed, and completing and reviewing the collection of information. Send comments regarding this burden estimate or any other aspect of this collection of information, including suggestions for reducing this burden, to Washington headquarters Services, Directorate for Information Operations and Reports, 1215 Jefferson Davis Highway, Suite 1204, Arlington, VA 22202-4302, and to the Office of Management and Budget, Paperwork Reduction Project (0704-0188) Washington DC 20503.			
1. AGENCY USE ONLY *(Leave blank)*	**2. REPORT DATE** March 2006	**3. REPORT TYPE AND DATES COVERED** Master's Thesis	
4. TITLE AND SUBTITLE: Development and Evolution of Cirrus in a Mesoscale Model			**5. FUNDING NUMBERS**
6. AUTHOR(S) Lewis, Michael M.			
7. PERFORMING ORGANIZATION NAME(S) AND ADDRESS(ES) Naval Postgraduate School Monterey, CA 93943-5000			**8. PERFORMING ORGANIZATION REPORT NUMBER**
9. SPONSORING /MONITORING AGENCY NAME(S) AND ADDRESS(ES) N/A			**10. SPONSORING/MONITORING AGENCY REPORT NUMBER**
11. SUPPLEMENTARY NOTES The views expressed in this thesis are those of the author and do not reflect the official policy or position of the Department of Defense or the U.S. Government.			
12a. DISTRIBUTION / AVAILABILITY STATEMENT Approved for public release; distribution is unlimited			**12b. DISTRIBUTION CODE**

13. ABSTRACT (maximum 200 words)

Cirrus cloud forecasting is of particular importance to various Department of Defense programs. This thesis takes a case study approach to study Air Force Weather Agency Mesoscale Model 5 (AFWA MM5) skill in forecasting cirrus clouds, which are not represented explicitly by the model (ice water mixing ratio is used as a surrogate.) Two cases are selected for study. For each case, an initial forecast time of interest is determined which serves as the beginning point for the case study. GOES data and 3-hourly MM5 data are then obtained at 3-hourly intervals to coincide with model forecast time steps between the initial time through the 30-hour forecast. A standard analysis is performed on all data to determine general atmospheric structure for each case at each 3-hourly point. Following this, the model's relative humidity with respect to ice, explicit ice water content, vertical velocity, and other fields are considered to determine if the model possesses the proper dynamical factors for cirrus formation. Finally, model coverage of ice cloud is compared to the ABL cloud mask results to determine how well the model's ice cloud forecasts verify against each 3-hourly observed ice water field taken from the GOES data.

Results indicate that the MM5 underforecasts cirrus coverage, and that the 90% relative humidity field with respect to ice may be a better approximation of observed cirrus coverage than the ice water field.

14. SUBJECT TERMS Cirrus, MM5, Mesoscale Model, Laser, ABL, Satellite, GOES			**15. NUMBER OF PAGES** 80
			16. PRICE CODE
17. SECURITY CLASSIFICATION OF REPORT Unclassified	**18. SECURITY CLASSIFICATION OF THIS PAGE** Unclassified	**19. SECURITY CLASSIFICATION OF ABSTRACT** Unclassified	**20. LIMITATION OF ABSTRACT** UL

NSN 7540-01-280-5500 Standard Form 298 (Rev. 2-89)
Prescribed by ANSI Std. 239-18

THIS PAGE INTENTIONALLY LEFT BLANK

Approved for public release; distribution is unlimited

DEVELOPMENT AND EVOLUTION OF CIRRUS IN A MESOSCALE MODEL

Michael M. Lewis
Captain, United States Air Force
B.S., University of South Alabama, 1997

Submitted in partial fulfillment of the
requirements for the degree of

MASTER OF SCIENCE IN METEOROLOGY

from the

NAVAL POSTGRADUATE SCHOOL
March 2006

Author: Michael M. Lewis

Approved by: Wendell A. Nuss
Thesis Advisor

Phillip A. Durkee
Second Reader

Phillip A. Durkee
Chairman, Department of Meteorology

THIS PAGE INTENTIONALLY LEFT BLANK

ABSTRACT

Cirrus forecasting is of particular importance to various Department of Defense programs. This thesis takes a case study approach to study Air Force Weather Agency Mesoscale Model 5 (AFWA MM5) skill in forecasting cirrus clouds, which are not represented explicitly by the model (ice water mixing ratio is used as a surrogate.) Two cases are selected for study. For each case, an initial forecast time of interest is determined which serves as the beginning point for the case study. GOES data and 3-hourly MM5 data are then obtained at 3-hourly intervals to coincide with model forecast time steps between the initial time through the 30-hour forecast. A standard analysis is performed on all data to determine general atmospheric structure for each case at each 3-hourly point. Following this, the model's relative humidity with respect to ice, explicit ice water content, vertical velocity, and other fields are considered to determine if the model possesses the proper dynamical factors for cirrus formation. Finally, model coverage of ice cloud is compared to the ABL cloud mask results to determine how well the model's ice cloud forecasts verify against each 3-hourly observed ice water field taken from the GOES data.

Results indicate that the MM5 underforecasts cirrus coverage, and that the 90% relative humidity field with respect to ice may be a better approximation of observed cirrus coverage than the ice water field.

THIS PAGE INTENTIONALLY LEFT BLANK

TABLE OF CONTENTS

LIST OF FIGURES

THIS PAGE INTENTIONALLY LEFT BLANK

LIST OF TABLES

THIS PAGE INTENTIONALLY LEFT BLANK

ACKNOWLEDGMENTS

I would like to thank my advisor, Professor Wendell A. Nuss of the Department of Meteorology, Naval Postgraduate School, for his guidance and support during the development of this thesis. His meteorological expertise and programming skill were critical in the analysis and processing of satellite and model data related to this thesis.

I would also like to thank Professor Philip A. Durkee for providing his knowledge regarding cloud mask techniques and various methods of cloud mask application

Mr. Don Norquist, Air Force Research Lab, and Mr. Gary Gustafson, AER, Inc., have been instrumental in providing the GOES satellite data and cloud mask results used in the case studies contained in this thesis. Their support was instrumental in getting the initial phase of this thesis completed. Mr. Robert Creasey, staff meteorologist, Naval Postgraduate School, also deserves my gratitude for providing critical data gathering and data management assistance. Also, Dr. Jerome Schmidt, Naval Research Laboratory, Monterey was gracious enough to take the time to describe the Reisner mixed phase ice microphysics scheme.

Finally, I want to thank my wife, Elizabeth, for her encouragement and support during this thesis writing effort.

THIS PAGE INTENTIONALLY LEFT BLANK

I. INTRODUCTION

Mesoscale models have long been in use for operational weather forecasting, yet verification of cirrus cloud forecasts by such models has received relatively little attention compared to verification of other sensible weather phenomena near the surface such as wind gusts, coastal jets, and precipitation. There are several reasons this is the case: verification of weather near the surface is relatively easy due to the higher number of surface weather reporting sites; detection of surface-based features is relatively inexpensive; and sensible weather at the surface has an effect on a wider number of people and missions and is therefore of greater interest than verification of weather effects aloft. Additionally, as more observing sites become automated, the inability of automated stations to report clouds above 12,000 feet results in fewer stations reporting high clouds. When mission-impacting weather is considered, we generally do not think of cirrus, because cirrus clouds do not adversely affect most day-to-day activities.

Cirrus' effects are not often considered important for most of our routine activities, but cirrus can have a profound effect on laser propagation. Understanding these impacts, and knowing where cirrus will be and in what amounts, is critical in providing accurate support to various Department of Defense (DoD) programs that rely on lasers. Such programs include the Transformational Communications Architecture (TCA) and the Airborne Laser (ABL) Program, as well as other projects of the High Energy Laser Joint Technology Office.

The uncertain nature of basic weather forecasting further complicates forecasting the development, presence, and movement of clouds. Many variables affect the development and movement of clouds (available moisture, dynamics, microphysics, etc.) and there are almost infinite combinations of these variables that can affect clouds in a model. A given amount of moisture in an area may assist development of cirrus in that area on one day, but may be insufficient for cirrus formation on a different day with different atmospheric dynamics. Importantly, many dynamical and microphysical processes involved in cloud formation are not fully represented in models. Such processes occur on a scale that is well below the model's ability to explicitly resolve

them; therefore parameterizations are developed that attempt to account for these processes. Parameterizations, however, cannot account for all the details necessary to provide accurate forecasts due to their lack of proper representation of microphysical processes.

Despite the challenges posed to cloud forecasting, MM5 model results are used in notional mission planning forecasts for the programs mentioned above, and similar model forecasts will be of continued importance for those programs as well as future laser-related operations. The Air Force Research Lab proposed this thesis research topic to address the issue of mesoscale model verification of cirrus cloud forecasts.

A. BASIS FOR THIS STUDY

Although not directly related to the meteorological details of this thesis, Ou (2002) provides some of the background as to why accurate model predictions of cirrus clouds are important when laser-related operations are considered. Ou (2002) developed a model to study the effect of backscattering on laser propagation through cirrus clouds, with an ABL-centric mindset. He found that laser transmission uncertainty due to cirrus particle size and orientation is negligible, but optical depth of cirrus coverage can greatly affect laser transmission uncertainty. From observation of cirrus, we know that cirrus clouds are not homogeneous with respect to optical depth. Ou (2002) tested two cases using homogeneous clouds before comparing those results to a scenario that involved real-world satellite data representative of inhomogeneity within cirrus.

The first model run was done for an aircraft above cloud level with backscattered and target-reflected power as functions of target height. Ou (2002) found that backscattered power is virtually constant near the aircraft, regardless of cloud optical depth, and that target-reflected power is initially much less than the power returned via backscattering. As the target left the surface, reflection of laser energy incident upon the target increased due to decreasing absorption with height by water vapor in the atmosphere. Target reflection decreased as the target approached and entered the clouds due to increasing optical depth. Once the target left the top of the cloud, reflected energy from the target increased to its maximum value.

For an aircraft within the clouds, backscattering was dominated by the contributions to backscattering made by the cloud ice particles near the aircraft. Ou (2002) found that backscattered energy was one to two orders of magnitude larger than for the aircraft flying outside of clouds. The effects of absorption, due to cloud particle scattering, aerosol presence, and air molecules, were small. Ice crystal shape and distribution greatly affected backscattered power. When the target was below cloud level, reflected energy was miniscule when cloud optical depth was 0.2 and was still quite small when below a cloud with optical depth of only 0.05. Approaching, within, and departing the cloud, the target reflection reached a minimum. Once above the cloud, the target reflected more and more energy as atmospheric water vapor decreased with altitude.

After running his model using homogeneous cases, Ou (2002) ran a comparison simulation for the case of inhomogeneous cirrus using observed satellite data to deduce mean effective ice crystal sizes from a cirrus case observed in northern Oklahoma on 18 April 1997. Ou placed the aircraft at 11.2 km altitude, 0.1km above cloud top. The cloud base was at 7.5 km, and the target began its ascent from the surface. As with the homogeneous cases, reflectance of the target increased as it departed the surface, up to a maximum sub-cloud value approximately halfway between the surface and the cloud base. Values of direct transmission below 4 km were slightly larger for the inhomogeneous cirrus event than for the modeled homogeneous event due to the along-beam optical depth being shorter for the inhomogeneous cloud. Between 4 km and cloud base level, direct transmission was slightly larger for the homogeneous case because of the smaller laser beam path through the homogeneous cloud. Although differences in transmittance and backscattering were relatively small outside of clouds, scattering and direct transmission were both significantly larger when the aircraft was located within the modeled homogeneous cirrus region due to the larger laser beam path as well as the smaller ice crystal size compared to the case of inhomogeneous cirrus. Below cloud level, inhomogeneous cirrus had a very small effect on laser transmission and backscattering.

Ou's (2002) results show that, for cirrus observed under realistic conditions, a missed cirrus forecast can result in ABL mission failure. The presence of unforecast

cirrus can significantly reduce laser transmission between aircraft and target, rendering the ABL useless in thwarting a threat, or leaving other laser systems inoperable.

B. OBJECTIVES

This study seeks to evaluate the AFWA MM5's ability to accurately forecast cirrus coverage over a 2-dimensional area from a starting time of interest up to the 30-hour forecast period. The study endeavors to obtain a basic understanding of model strengths and weaknesses in forecasting ice clouds for weather events a forecaster would experience on a routine basis.

Specific goals of this study are to:

1. Determine whether cirrus forecast errors are mostly due to basic weather system forecast errors (e.g., timing or phase errors) or cloud process errors;

2. Assess how model dynamics, moisture distribution, and cloud microphysics contribute to cirrus formation in the model;

3. Identify possible limitations in MM5 cloud parameterizations that impact on cirrus forecast accuracy;

4. Identify critical parameters that might help predict cirrus even when explicit model forecasts do not report ice water for a given area.

II. BACKGROUND/LITERATURE REVIEW

A. CHARACTERISTICS OF CIRRUS

It is important to define what is meant by cirrus, what synoptic features typically drive cirrus formation, and what conditions (not synoptically-driven) can result in the formation of cirrus.

1. Composition

Cirriform clouds are composed almost entirely of ice crystals that form from the freezing of supercooled water droplets. Three genuses of high clouds exist: cirrus (cirriform appearance), cirrostratus (stratiform appearance), and cirrocumulus (cumuliform appearance).

Cirrus clouds are commonly known as "mares' tails", and appear as strands or filaments of clouds due to advection of ice crystals downstream by high winds aloft. Stratiform and cumuliform clouds appear as patches; cirrostratus has a smooth appearance, while cirrocumulus has a bumpy appearance. Within each genus, several species and varieties exist that further define cloud characteristics. This study will use the term, "cirrus" to generally refer to ice clouds, regardless of genus.

2. Location and Related Synoptic-Scale Features

In mid-latitudes, cirriform clouds are normally found between 20,000 to 30,000 feet. It is not uncommon to find cirriform clouds below 10,000 feet in polar areas and as high as 60,000 feet or more in the tropics.

Cirriform clouds are typically associated with various synoptic conditions: in advance of warm fronts, "spilling over" ridges, associated with jet streams, and lee of mountain ranges. Related dynamical details as applicable to the case studies in this document are provided in the next section.

3. Formation Conditions and Basic Governing Dynamics

Development of cirriform clouds first requires cooling a parcel of air to saturation, usually by gentle lifting along an isentropic surface. Following saturation, the nucleation phase occurs by one of two mechanisms: heterogeneous nucleation or homogeneous nucleation. Heterogeneous nucleation requires a catalyst or ice nucleus and typically occurs when temperatures range between -5 degrees Celsius to

approximately -40 degrees Celsius depending on the availability of ice nuclei. Ice nuclei generally take the form of dust particles or preexisting ice particles. Homogeneous nucleation occurs at temperatures near -40 degrees Celsius and does not require the preexisting presence of ice nuclei. According to Houze (1993), cirrus can exist down to -85 degrees Celsius. Typical vertical velocity values for the formation of cirrus are on the order of 0.1 to 0.2 m s^{-1} in most cases, although formation of certain convective species of cirrus is associated with vertical velocity values of 1 to 2 m s^{-1}. During the FIRE cirrus experiments, Starr and Lare (1993) observed cirrus in areas of vertical velocity values on the order of 0.02 m s^{-1}.

Cirrus clouds are typically located ahead of surface warm fronts where warmer air at low levels rises, cools adiabatically, and eventually condenses. Following saturation, continued cooling leads to the formation of ice crystals via one of the two methods presented above.

This thesis will focus on two cases of interest. In the first case the cirrus initially resulted from the lifting of moisture by convection in the tropics, which then streamed into northern Mexico and the desert southwest by the forcing of an upper-level ridge to the east and an upper-level closed low off the United States west coast. In the second case, cirrus were formed by lifting ahead of an upper level low. These cirrus clouds moved across an upper-level ridge downstream of their initial moisture source. In lieu of a method to directly observe model parameterization details as time progresses, this thesis will investigate the dynamics responsible for cirrus formation in both cases and attempt to draw conclusions regarding how well the MM5 places cirrus related to modeled dynamical forcing.

4. Microphysical Properties

As described by Houze (1993), cirriform clouds typically possess ice contents on the order of 0.001 to 0.25 g m^{-3}, with the most typical values on the order of 0.01 to 0.1 g m^{-3}. Particle sizes range from 50 to 1000 μm. A variety of shapes can describe the ice crystals that compose cirrus clouds, including columns, bullets, bullet-rosettes, and plates. Aggregates of the various crystal shapes are fairly common, since partially melted ice crystals do occasionally re-freeze upon making contact with frozen crystals (i.e., heterogeneous nucleation.)

B. CLOUD MASK THEORY

The cloud mask used by the ABL was developed by Atmospheric and Environmental Research Incorporated (AER). The algorithm makes use of a variety of tests to determine cloud coverage and phase using various data sources. These data sources include (among others) the Air Force Weather Agency Mesoscale Model 5 (AFWA MM5), the Geostationary Operational Environmental Satellite (GOES), and the Moderate Resolution Imaging Spectrometer (MODIS) satellite. In addition to cloud tests, background tests are also conducted to determine the presence of sun glint, desert backgrounds, and snow/ice backgrounds. Knowledge of background conditions is critical to successful results from certain cloud tests.

Although data from the MODIS hardware can also be used, the cloud mask for this thesis was run strictly on GOES satellite data (specifically, GOES-10.) The GOES-10 imager contains sensors centered at the 0.65, 3.9, 6.7, 10.8, and 12.0 μm wavelengths. The GOES-12 imager also has the 0.65, 3.9, 6.7, and 10.8 μm wavelengths in the first four channels, however the 12.0 μm band is no longer present, and a 13.0 μm band has been added. The descriptions below regarding test theory and the various cloud tests are applicable to GOES-10 data, as the difference in the last GOES-12 band's wavelength requires some algorithm changes to the cloud mask that degrade accuracy of the cloud mask, principally in terminator regions (AFRL, 2001.)

1. Remote Sensing Theory

An understanding of basic satellite remote sensing theory is necessary before discussing the cloud tests, which rely upon various results from reflectance channels and emittance channels. Table 1.1 describes the satellite wavelengths used by the cloud mask tests, and the associated satellite system and resulting calibrated quantity.

Table 1.1. Sensor channel wavelengths used by the AER cloud mask algorithms. Wavelength Designations: VIS-visible, NIR-near infrared, SWIR-shortwave infrared, MWIR-mid-wave infrared, WV-water vapor, LWIR-long wave infrared. EBBT: Equivalent Blackbody Brightness Temperature. From AFRL-VS-TR-2001-1549, p. 3.

Wavelength (μm)	Designation	GOES Imager	AVHRR	MODIS	Calibrated Quantity
0.65	VIS	X	X	X	Reflectance
0.85	NIR		X	X	Reflectance
1.38	SWIR			X	Reflectance
1.60	SWIR		X	X	Reflectance
3.70 – 3.90	MWIR	X	X	X	EBBT
6.70 – 7.00	WV	X		X	EBBT
8.55	LWIR			X	EBBT
10.8	LWIR	X	X	X	EBBT
12.0	LWIR	X	X	X	EBBT

a. Reflectance Channels

Reflectance properties for different surfaces vary with wavelength in the visible and near-infrared (NIR) bands. Water surfaces are poor reflectors in the NIR portion of the electromagnetic spectrum, whereas land surfaces are poor reflectors in the NIR except for at approximately 0.86 μm. Clouds, on the other hand are generally good reflectors in the NIR, except for ice clouds, which do not reflect well at 1.6 μm. Ice and snow exhibit peak reflectance at 0.65 μm and 0.85 μm. Taken together, these observations allow for automated discrimination between cloudy areas and clear areas.

b. Emittance Channels

In addition to using the NIR portion of the electromagnetic spectrum for cloud tests, the cloud algorithm also uses infrared (IR) channels as shown in Table 1. At these wavelengths, energy measured by the satellite sensor is mostly due to the emittance and temperature of the surface or atmospheric constituent (e.g., clouds), the transmittance

of the atmosphere. Reflectance of cloud and background surfaces is negligible at these wavelengths.

It is important to note that the 12.0 μm channel is more strongly affected by atmospheric water vapor absorption than the 10.8 μm channel, and as a result the brightness temperatures obtained with this channel are slightly less than those obtained from the 10.8 μm channel. Also, we note that in the 8.55 to 10.8 μm bands, absorption by atmospheric water vapor is roughly the same but absorption due to ice particles increases with wavelength between 10.8 and 12.0 μm. As we will see, these are all important factors used by the cloud mask algorithm in determining cloud presence and phase.

c. Midwave Infrared Channel

The 3.9 μm channel is unique because it provides both reflected solar energy and emitted energy. This characteristic, along with the optical properties of clouds at this wavelength, is very useful for detecting clouds that have weak or ambiguous spectral signatures at the other wavelengths used by the cloud detection algorithm.

d. Water Vapor Channel

We know that strong water vapor absorption occurs in the atmosphere at 6.7 μm. Low-level features are masked out by this, resulting in resolution of only mid and high-level features. When cirrus optical depth is very small, transmission of background radiation through the cloud can reduce the cloud-background contrast to a level that is undetectable by automated cloud algorithms at visible, mid-wave IR, and long-wave IR wavelengths. This is especially true over bright and warm backgrounds such as deserts. Using data from the "opaque" 6.7 μm band, it is possible to develop a technique (see cloud test section below) to improve detection of thin cirrus over background conditions that stress traditional LWIR and visible techniques.

2. Cloud Tests

The cloud tests and background tests make use of the aforementioned satellite theory to determine if a given pixel is clear or cloudy, and the phase (ice or water) of cloudy pixels. Each test is performed by the cloud mask algorithm before final determination of cloud presence and phase is determined. Results from all tests are

considered jointly when assigning a clear or cloudy classification and cloud phase (if applicable) to a given pixel. The cloud detection tests are described below:

a. Thermally Distinct Cloud Test

Most clouds that are not very low in the atmosphere exhibit a significantly colder brightness temperature than their terrestrial background. The thermally distinct cloud test is a simple single LWIR channel threshold test that is designed to discriminate between the thermal signatures of obvious mid- and high-level clouds from the terrestrial background's thermal signature.

The test is not useful for highly transmissive cirrus (which can appear warmer than their true temperature), marine stratus and other low clouds, partially cloud-filled fields of view, and high-latitude snow/ice covered backgrounds. Each of these cases is addressed by other cloud tests.

This cloud test requires an estimate of the skin temperature over the region of interest so that corresponding clear-sky brightness temperatures can be computed. This skin temperature estimate is provided by a mesoscale model such as the AFWA MM5. As appropriate, a land-ice temperature model or a sea-surface temperature model is used to provide temperature data for ice and sea surfaces.

The cloud test requires that the LWIR brightness temperature at 10.8 or 12.0 μm be less than the predicted clear-scene temperature by an amount greater than the uncertainty in the clear scene estimate. The magnitude of the threshold is determined by accumulating statistics on the measured difference between satellite EBBTs and the skin temperature of pixels determined to be cloud-free by previous runs of the cloud algorithm. Statistics are kept in a rotating 10-day database according to satellite overpass time, location, and background geography type.

b. Single Channel Reflectance Test

This test discriminates relatively high cloud reflectance from a predicted background value in a similar manner to the thermal threshold test described above. Clouds typically have a higher reflectance than their terrestrial backgrounds at NIR wavelengths. To avoid difficulties associated with high reflectance values over some land surfaces at 0.86 μm and water surfaces under certain conditions at 0.65 μm, the

scheme considers only the results from the 0.86 μm band over water and the 0.65 μm band over land. In this manner, cloud contrast with the background surface is maximized. Separate thresholds are maintained for land backgrounds and water backgrounds. Limitations for this test include transmissive cirrus, high-albedo ecosystems, sun glint over water surfaces, desert, and snow/ice covered background conditions.

c. Near-IR/Visible Reflectance Test

This test is a ratio test that compares the relative magnitudes of 0.86 μm (NIR) and 0.65 μm (visible) reflectance values. Optically thick clouds generally exhibit a very similar spectral signature between the visible and NIR bands. For land and water surfaces, however, the spectral signatures between these two bands can vary significantly. The ratio of NIR to VIS reflectance can tell us a great deal about cloud cover.

A ratio of approximately 1.0 indicates the likely presence of cloud cover because surface features are effectively masked. A ratio that differs significantly from 1.0 indicates either vegetated land (in the case of a ratio greater than 1.0) or water (in the case of a ratio less than 1.0.) The thresholds between clouds/no clouds are determined empirically, and are adjusted as needed when conditions such as high humidity and high aerosol/haze concentration exist. The results of this test are only useful in the absence of sun glint, desert background, and snow/ice covered background conditions. Additionally, mixed geography types such as coastlines prevent use of this test.

d. Low Cloud and Fog Test

Low clouds and fog are typically virtually indistinct from their background surfaces in the LWIR, but show high contrast to their backgrounds at visible and NIR wavelengths during daytime. Low clouds and fog also have recognizable spectral signatures in the MWIR when compared to LWIR brightness temperatures. The low cloud and fog test is designed to supplement the visible and NIR test during daytime, and addresses the inability of the thermal cloud test to discriminate thermally indistinct clouds at night.

The magnitude of the MWIR-LWIR spectral differences for small water droplet clouds varies depending on time. During daytime, a cloud's reflectivity in the 3.9 μm band is greater than the LWIR brightness temperature for the cloud. At night, the

emissivity of a cloud measured in the 3.9 μm band is less than the LWIR-indicated brightness temperature. The sign of the signature changes from day (positive difference) to night (negative difference.)

This test maintains separate thresholds for desert, non-desert, and potential sun glint backgrounds due to the high reflectance within the 3.9 μm band of those features. Desert surfaces have a lower 3.9 μm emissivity at night than other terrestrial surfaces, so separate nighttime thresholds are maintained for desert areas.

3. Cirrus-Specific Cloud Tests

As the cloud detection tests have shown, cirrus (particularly thin cirrus) are often difficult to detect. Optically thick cirrus clouds are easily identified via temperature contrast with the background. However, cirrus clouds with nonzero transmittance are common, resulting in LWIR brightness temperatures that can be much greater than the actual cloud temperature. This can result in cirrus being erroneously classified as mid-level (water) clouds by automated classification schemes. The schemes described below help to improve detection of cirrus and ensure correct phase categorization. The AFRL (2001) technical report was used as a reference in preparing this section, and contains further details regarding each of the tests described below.

a. LWIR Cirrus Test

This test examines LWIR brightness temperature differences between 8.55, 10.8, and 12.0 μm. As discussed earlier, ice particle absorption increases with wavelength across this spectral region and water vapor attenuation is slightly stronger at the 12 μm wavelength. These factors result in cirrus brightness temperatures that decrease with wavelength.

The cloud detection threshold used for this test is defined as a function of atmospheric water vapor and path length through the atmosphere due to the fact that, given the factors described above, it is possible to obtain erroneous results due to atmospheric moisture in a clear scene. Additionally, over snow or ice-covered backgrounds, the test assumes that 10.8 μm brightness temperatures measured from the cirrus clouds are colder than the clear-scene terrestrial background by an amount greater than a defined threshold value.

b. NIR Cirrus Test

Optically thin cirrus can be detected using the Moderate Resolution Imaging Spectroradiometer (MODIS) in the 1.38 μm band. Here, water vapor absorption masks out reflected solar radiation from beneath clouds so that the contrast between cirrus clouds and the background is sufficient to allow for thin cirrus detection.

This test has difficulty over areas with high terrain relief (snow-covered mountains) and locations with very low atmospheric water vapor and reflective surfaces (polar areas.)

c. MWIR-LWIR Cirrus Test

The 12.0 μm channel is typically used for comparison with the 3.9 μm channel in this test because of ice particles' increased absorption at this wavelength compared to the 10.8 μm wavelength. In practice, however, there is little difference in the observed temperatures between the 10.8 μm and 12.0 μm wavelengths. As a result, the cloud signature obtained by differencing the 3.9-12.0 μm bands is only slightly less than the signature obtained by differencing the 3.9-10.8 μm bands is only slightly greater for the 3.9-12.0 μm band.

Use of the 12.0 μm channel, however, can result in errors that lead to false cloud detection when there is a clear scene with high humidity levels near the surface. In this situation, strong water vapor absorption near the surface causes the 12.0 μm equivalent blackbody temperature (EBBT) to appear much lower than the true temperature. To remedy this problem, the 10.8 μm data are used rather than the 12.0 μm data when integrated water vapor values in a column are greater than a defined threshold value.

d. Water Vapor Channel Cirrus Test

The 6.7 μm wavelength measures upwelling thermal radiation emitted by water vapor in the atmosphere. The magnitude of the 6.7 μm brightness temperature depends on the amount of water vapor present along the atmospheric path, but will be less than temperatures computed for the same scene at LWIR wavelengths in all but the driest of atmospheres. Any cloud in the field of view will reduce the difference between the 6.7 and 10.8 μm brightness temperatures since 10.8 μm brightness temperature will be representative of the ambient temperature at the cloud's level.

The water vapor channel cirrus test first determines known clear-scene areas, evaluates the 6.7-10.8 μm temperature differences for these areas, and then searches the scene for locations where the difference falls below a cutoff threshold based on the clear-scene difference. This test is advantageous because it does not require us to know surface characteristics, which in some cases may be difficult to obtain.

4. Cloud Phase Classification

In order to obtain cloud optical and microphysical properties, it is necessary for the cloud mask algorithm to discriminate between ice cloud and water cloud. The cloud tests above use spectral signatures that can represent either ice cloud or water cloud, so phase discrimination is still necessary.

The phase test uses spectral signatures representative of ice cloud to classify the phase of pixels identified as cloudy by the aforementioned tests. If a pixel fails to meet ice cloud spectral signature requirements, it is classified as a water cloud pixel. The phase determination is made by applying several tests, as described below.

a. LWIR Brightness Temperature Test

Pixels are tested to see if their brightness temperature value allows them to be unequivocally classified as ice cloud. Any pixel with a brightness temperature less than 233K is classified as ice cloud.

b. MWIR-LWIR Test

A positive MWIR-LWIR difference (at night) is unique to transmissive cirrus for reasons described above.

c. NIR Test

During daytime, if the NIR thin cirrus test detects cloud and the other reflectance tests do not, then the pixel is classified as ice cloud.

d. Brightness Temperature Difference Test

Due to the nearly uniform increase in particle absorption with wavelength in the LWIR, coupled with the preferential increase between 10.8 and 12.0 μm for water droplets, an 8.55-10.8 μm BTD greater than a 10.8-12.0 μm BTD difference is indicative of ice cloud, while an 8.55-10.8 μm BTD less than a 10.8-12.0 μm BTD is indicative of water cloud.

C. AIR FORCE WEATHER AGENCY MESOSCALE MODEL 5

The Mesoscale Model 5 (MM5) was developed by the National Center for Atmospheric Research (NCAR) and the Pennsylvania State University. The MM5 was declared operational for Air Force use in 1997 by the Air Force Weather Agency (AFWA), and is tailored as necessary by AFWA to perform as well as possible in every theatre in which it is run. Various physics packages determine how the model treats various atmospheric processes such as convection, cloud moisture phase changes, etc. Certain parameters contained in the physics packages can be adjusted by modelers at AFWA to ensure the most favorable configurations are used.

The MM5 implementation used in this thesis is the 15km AFWA MM5. This model contains 42 sigma levels, with highest vertical resolution near the surface and decreasing vertical resolution as we travel toward the top of the modeled atmosphere at 50mb. This is a critical factor when considering cirrus forecasting within the model. Since cirrus are often only a few meters thick, their location and ice water concentration may not be accurately represented by the model. Various papers have studied the problem of forecasting cirrus using a mesoscale model. Starr and Wylie (1990) found that vertical resolution of 0.5 km or better is probably required to adequately resolve dynamical forcing required for the development of a physically-based model parameterization of cirrus.

The problem of forecasting cirrus within a numerical model is an extremely difficult and complex task. Forecasting of cirrus goes well beyond simply knowing where cirrus are initially located and advecting the clouds properly. Not only must the model account for the movement and development of cirrus, it must also account for development related to microphysical processes that occur many orders of magnitude below the model's resolution. These cloud microphysical processes are represented within a forecast model by any one of several parameterizations. The AFWA MM5 uses a modified Reisner mixed-phase scheme. Due to the tendency to overforecast ice, the scheme as implemented in the AFWA MM5 does not account for riming processes or graupel processes when computing ice water mixing ratio.

Norquist and d'Entremont. (2003) have used explicit ice water content to represent cirrus in MM5 output. The ice water mixing ratio field output by the model is the result of many calculations for each model gridpoint, and is dependent on several factors. Equation 1 shows the ice water mixing ratio formula as given by Reisner:

$$\frac{\partial p * qi}{\partial t} = -ADV(P * q_i) + DIV(P * q_i) + D(q_i) + p * (P_{idsn} + P_{ifzc} + P_{ispl} + P_{idep} + P_{i.iacw} - P_{icng} - \mathrm{P}_{\mathrm{r}aci} - P_{saci} - P_{icns} - P_{imlt}) \quad (1)$$

It is convenient to view handling of ice water mixing ratio in the model in terms of sources and sinks (Reisner, 1998). Table 2.1 categorizes the production terms in the equation above into sources and sinks. Items listed in Reisner's equation that are not included in the AFWA MM5 are P_{icng}, $P_{i.iacw}$, and P_{raci}.

Table 2.1. Terms comprising the Reisner mixed-phase ice microphysics scheme. Shaded areas indicate scheme terms that do not apply to the AFWA MM5 implementation of the scheme.

Source Terms	**Sink Terms**
P_{idsn}: Initiation of nucleation	P_{saci}: Snow generation due to collection of ice by snow
P_{ifzc}: Heterogeneous and homogeneous freezing of cloud drops	P_{icns}: Total conversion of cloud ice to snow
P_{ispl}: Increase in mass of cloud ice associated with ice multiplication	P_{imlt}: Cloud water generation by the melting of ice
P_{idep}: Depositional growth of cloud ice	P_{icng}: Conversion of cloud ice to graupel
$P_{i.iacw}$: Contribution of riming to ice production	P_{raci}: Graupel generation by collision of ice and cloud water

Reisner expresses initiation of ice nucleation as a function of the number of ice crystals forecast at a particular gridpoint versus the number of ice crystals already present at that gridpoint. The initial number of crystals at a gridpoint is empirically determined

using Fletcher's curve (Fletcher, 1962) and temperature data taken from the model. The scheme is known to overpredict ice crystal concentrations for very low temperatures, so the lowest temperature is limited to 246 K. If the number of ice crystals predicted by the Fletcher curve is greater than the number of ice crystals already present at a given gridpoint, the additional vapor at that gridpoint is used to generate ice crystals until the predicted number and actual number match, at a rate determined by the first source term listed in the table above. With a known number of ice crystals, the model can now calculate the rate of vapor depositional growth of cloud ice, which depends on the extent of supersaturation, mean crystal size or mass, and the number of ice crystals. Vapor transfer rates for riming and graupel processes are neglected by the AFWA MM5. Additionally, the MM5 normalizes vapor deposition rates so that over depletion of vapor and subsaturation (associated with latent heat release) do not take place.

The model computes the results for each process identified in the table above based upon formulas (reference NCAR Technical Note TN-398+STR for details), and uses those results as part of its process to determine results for the ice water mixing ratio field. There are many uncertainties involved in the computation of ice water values for a given location. For instance, determination of the number of particles at a given location, based on statistically-determined particle concentration, is a source of error for heterogeneous nucleation. Temperature thresholds for homogeneous nucleation are uncertain, and this temperature uncertainty can contribute to errors in the forecast number of particles at a gridpoint. Minus 40 C is the value used by the MM5 to represent the onset of homogeneous nucleation; however homogeneous nucleation may occur at slightly warmer temperatures around minus 38 C in the real atmosphere.

THIS PAGE INTENTIONALLY LEFT BLANK

III. METHODS AND PROCEDURES

A. ANALYSIS METHOD

Cases selected for this study are typical for day-to-day forecasting operations. Cases were selected by observing infrared satellite loops for periods of significant cirrus field development and/or evolution. The focus for each case is the 18-30 hour forecast period, so cases were selected so that the time of the initial image coincided with the 18-hour forecast time of the MM5 run that was valid at the time the case began.

The MM5 provides forecast output for each 3-hour point within the period of interest, so satellite and model data were also compiled at times corresponding to the MM5's 18, 21, 24, 27, and 30 hour forecast periods. The Naval Postgraduate School Meteorology department typically receives GOES satellite data via FTP from the Naval Research Laboratory, Monterey and 15km MM5 pressure and sigma level data are routinely received from the Air Force Weather Agency for select forecast hours from each model run.

Once all satellite images for each case were saved, the ABL cloud mask processing code was applied to the images and merged with the image data. Proprietary scripts were used to place these data into a form useful by other routines that arranged the data into a format that could be studied along with model output within GEMPAK/GARP (General Meteorology Package / General Analysis and Rendering Program) software.

B. CASE STUDY MODEL VERIFICATION METHOD

In order to gain an understanding of how the MM5 forecast predicted the basic atmospheric structure from the case study start time through the 30-hour forecast, the observed Global Forecast System (GFS) analyses were used to verify the intensity, placement, and movement of significant features. The GFS analyses were chosen to verify the MM5 due to their increased availability versus subsequent MM5 model analyses which are only available every 12 hours. This allowed for direct verification of the MM5 more frequently during the study period for each case. Height and wind fields at various levels were considered in the verification and only areas where significant

deviation between the GFS and MM5 occurred are shown in the figures associated with each case.

To assess the model dynamics, moisture, and cloud distributions, the MM5 forecasts were compared to the satellite-derived cloud mask. This was done using GARP to overlay relevant fields. Position and phase errors in the model forecasts—particularly with the first case study—prevented direct comparison of the model ice field to observed cirrus clouds, but the characteristics of the model clouds and associated dynamic forcings were still useful to help understand how the model generated the clouds.

IV. CASE STUDY I: UPPER-LEVEL CLOSED LOW

A. CASE DESCRIPTION

This case focused on a closed upper-level low moving toward the western United States on 21 October 2005. The low had no jet support, and moved very slowly to the east during the study period. Figures 4.1.a through 4.1.e show the evolution of the cirrus field from 21/00Z through 21/12Z. The cirrus field at the beginning of the case study was mostly located over the Pacific, and was the result of convection over the tropics the day before the case study began. The cirrus field subsequently entered an area of increasing difluence between an upper low to its north and a ridge to its east that acted to spread out the cirrus at the northern extent of the plume. Additionally, large-scale upward motion in the difluent region resulted in the development of new cirrus. Some of the cirrus clouds were pulled downstream, to the east, around flow related to the ridge. Other cirrus clouds were drawn around the upper low by the end of the period.

B. MM5 FORECAST VERIFICATION

The GFS analyses from 21 October at 0000Z, 0600Z, and 1200Z were used to verify the corresponding 18, 24, and 30-hour forecasts from the 20 October 0600Z MM5 run. Verification was performed for wind and height fields at 300, 400, and 500mb to determine how well the model replicated the cirrus-level transport winds.

Generally, forecast errors in the wind speed field were minimal but significant errors were present in the height field by the 18 hour forecast period. The errors present in the height field at the 18 hour forecast period persisted through the end of the case study. Figure 4.2.a shows the 18-hour MM5 height forecast verification at 300mb. The height of the low is deeper in the GFS analysis than for the MM5 forecast, and the ridge over the interior of Mexico is represented more strongly in the GFS than the MM5. Most significantly, however, the MM5 misses the sharpness of the ridge axis across Mexico and the desert southwest. The result of these height errors is to produce flow that is more zonal in the MM5 output than is observed. Consequently the actual cloud field (shown in Figures 4.1.a through 4.1.e) appears to agree better with the GFS analyzed height field with its more north-south orientation. In addition, directly ahead of the low, the GFS indicates much stronger difluence taking place than is occurring in the MM5. This

analyzed difference in the GFS is consistent with the fanning out of the cirrus field shown in Figures 4.1.c through 4.1.e. While the MM5 shows some difluence, it tends to be less and is located in a different area than the observed cirrus. Therefore, the MM5 cirrus forecasts associated with this process are characterized by significant placement error.

The MM5 wind field (not shown) indicated a jet feature around the base of the low that extends through southern Arizona, central New Mexico, and across northern Texas. This band of higher winds is located just to the north of the modeled cirrus coverage, and is typical of cirrus forced by an anticyclonically curved jet.

Figure 4.2.b shows the 24-hour MM5 forecast compared to the GFS analysis valid at 06Z on 21 Oct 05. The height pattern remains similar to what is shown in Figure 4.2.a, with the GFS showing a much more marked ridge across the desert southwest than the MM5. The height discrepancies are more evident at mid-levels for this forecast period, which indicates the MM5 is beginning to deviate more from observed conditions. The MM5 continues to underforecast the depth of the low near the west coast and intensity of the ridging east of the low. The differences in extent of the ridge axis are particularly evident across central Arizona into southern Nevada, which is where the observed cirrus shown in Figure 4.1.c is beginning to spread out.

As Figure 4.2.c shows, the GFS continues to analyze a deeper low at 300mb at 21/12Z than the 30-hour forecast from the MM5. This trend was found at lower levels as well. The GFS also continues to analyze a sharper ridge across the desert southwest and northern Mexico than forecast by the MM5. The GFS and MM5 placements of the low center between 300mb and 500mb (not shown) agree very well, as has been the case throughout the entire period of interest. This indicates that the MM5 is moving the low appropriately despite weak synoptic-scale support for its movement. Given the GFS upper air height pattern, the analyzed GFS winds at 200mb, 300mb, and 500mb are from a more southerly direction ahead of the low as noted earlier, and the height pattern overall remains more conducive to stronger divergence (and greater cloud coverage) ahead of the low than the forecast by the MM5 indicates.

C. ANALYSIS

The upward motion and ice water mixing ratio were examined to determine the relationship between the dynamics and the model-produced cirrus clouds. Case I is characterized by strong upward vertical motion aloft in the difluent area ahead of the closed low, and strong upward motions streaming eastward across northern Mexico, as shown in Figures 4.3.a through 4.3.e. The main band of ice water mixing ratio values began at approximately 1725 sigma and continued to about 3190 sigma (approximately 170mb to 320mb), although there were occasional small areas of ice water mixing ratio values above 1725 sigma. The ice water field gradually diminished below 3190 sigma.

The 2880 sigma level, approximately 280mb, was chosen as the representative sigma level for the modeled cirrus field for this case. Normally cirrus are expected in areas of fairly weak upward motion, and indeed there is a strong correlation between upward motion and the presence of ice water in the model at 2880 sigma as indicated in Figure 4.3.a through 4.3.e. (Note: vertical motions are taken from the 300mb level but are representative of vertical velocities within the main cirrus band at all levels where it is found.) However, there is also a strong correlation between the 2880 sigma cirrus field and moisture divergence, as shown in Figures 4.4.a through 4.4.e. The correspondence between moisture divergence and presence of ice water mixing ratio values at the 2880 sigma level shows that the model ice must be continually created to offset the moisture divergence. The creation process is the upward motion from below of nearly saturated air (with respect to ice) that freezes into ice as it cools. Critical to maintaining cirrus of this type in the model is the supply of nearly saturated air in the slowly rising plume. If this diminishes, the model clouds may dissipate too soon.

Interestingly, subjective analysis showed that the amount of ice coverage at the upper sigma levels in and near the top of the band diminished with time, particularly after the 06-hour forecast, while the amount of ice coverage at lower levels increased. The system does become less organized with time, and this is likely a reflection of diminishing support for cirrus formation as upward motions and, consequently, support for large-scale supersaturation subside. The decrease in organization of model ice also is evident in the observed cirrus fields (Figures 4.1.a through 4.1.e.)

In general, the ice water tends to coincide with regions of relatively strong upward motion (shaded areas in Figure 4.3.a through 4.3.e.) The broad area of upward motion ahead of the low over northern Baja produces no ice water in the model. The lack of ice water in this region is presumably due to the fact that the moisture source for the ice water does not flow into this region.

Additionally, Figures 4.5.a through 4.5.e indicate that the upward vertical velocity fields lie within areas of strong frontolysis. Again, this was an unexpected result. As time passes, however, the cirrus field dissipates due to weakening of the low and ongoing frontolytical forcing. It appears that this frontolytical forcing provides an inverse thermal circulation, which results in slight warming of air within the cirrus field and therefore causes a decrease in relative humidity with respect to ice over time.

D. RESULTS

To verify the model's cirrus forecast, the ice water field composite for all levels where ice water was present in the model was plotted versus the corresponding cloud mask results from 21/00Z through 21/12Z as shown in Figures 4.6.a through 4.6.c. It is evident that the ice water field is dissipating with time, which agrees well with the frontolytical forcing evident in Figures 4.5.a through 4.5.e. Significant phase errors were present from the 18 hour forecast through the 30 hour forecast. As described earlier, this was a result of the MM5 under-forecasting the ridge sharpness, and as a result under-forecasting the location of cirrus as well as the strength of divergent flow across Arizona which led to significant cirrus coverage there. Finally, overall cloud coverage was less than observed via the cloud mask results, particularly later in the forecast period when the MM5 began to forecast diminished frontogenesis and upward vertical motions along the main cirrus band over northern Mexico and the southern United States.

The ice field shown in Figures 4.7.a through 4.7.c was examined to determine whether the underforecast of model cirrus might be due to a lack of moist air to feed the clouds. Again, our ice water field was becoming more diffuse with time, but the satellite images in Figure 4.1.a through 4.1.e show that the observed cirrus pattern remained relatively intact with time. Importantly, the 90% relative humidity over ice (shaded green) appears to fit the observed cirrus pattern better than the ice water mixing ratio composite when model phasing error is taken into account. This suggests that the

moisture supply was sufficient but the dynamic forcing was not sufficiently strong to produce enough cirrus in the model. The model may require too much vertical motion to initiate and maintain ice clouds, which contributes to its underforecast of cirrus that is observed in the real atmosphere accompanying far lower vertical velocities.

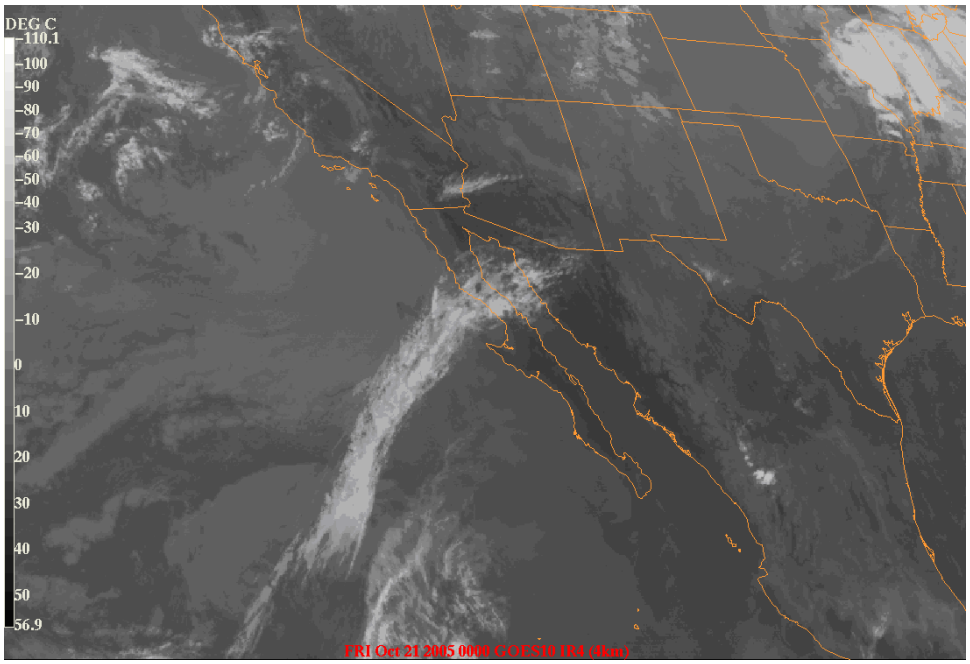

Figure 4.1.a. GOES-W image valid at 21 Oct 05/00Z.

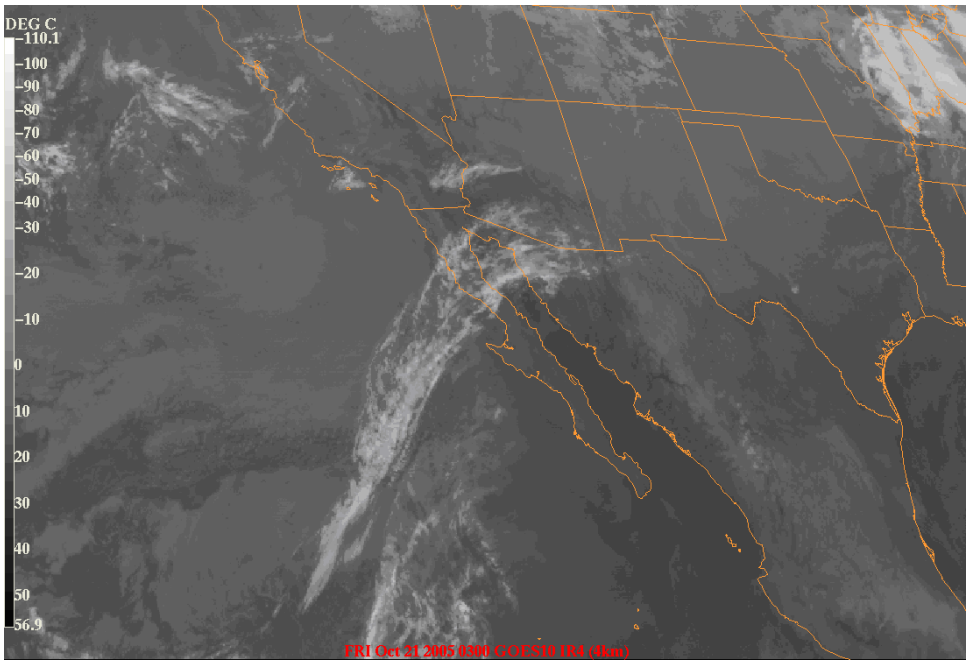

Figure 4.1.b. GOES-W image valid at 21 Oct 05/03Z.

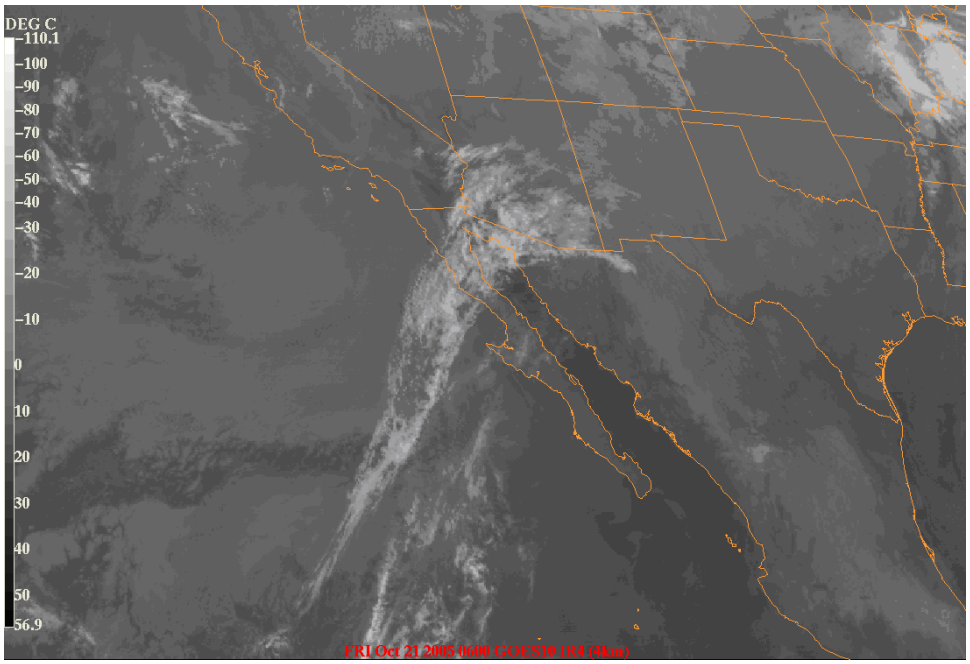

Figure 4.1.c. GOES-W image valid at 21 Oct 05/06Z.

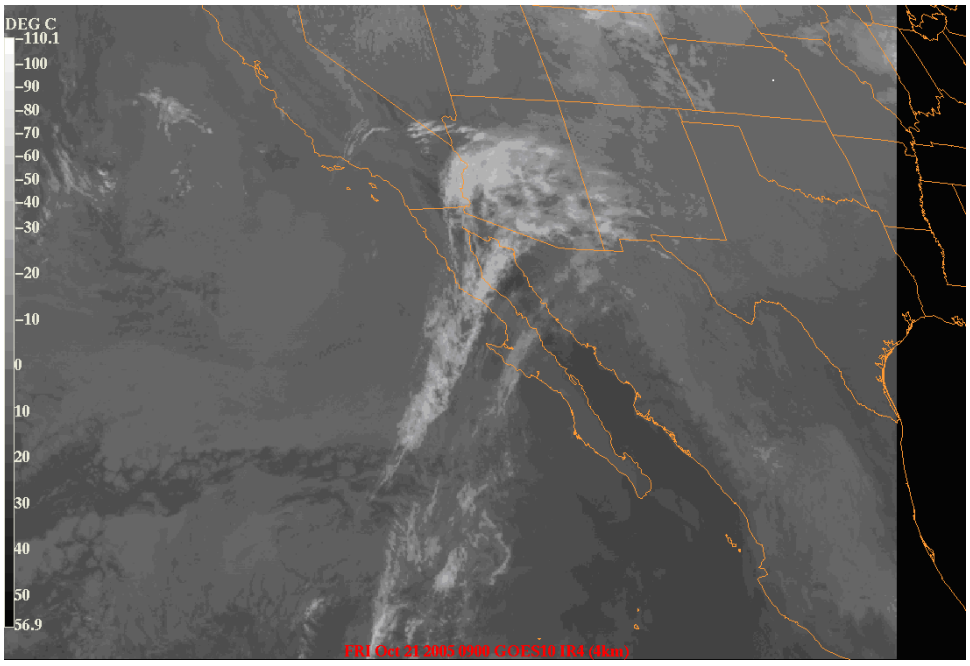

Figure 4.1.d. GOES-W image valid at 21 Oct 05/09Z.

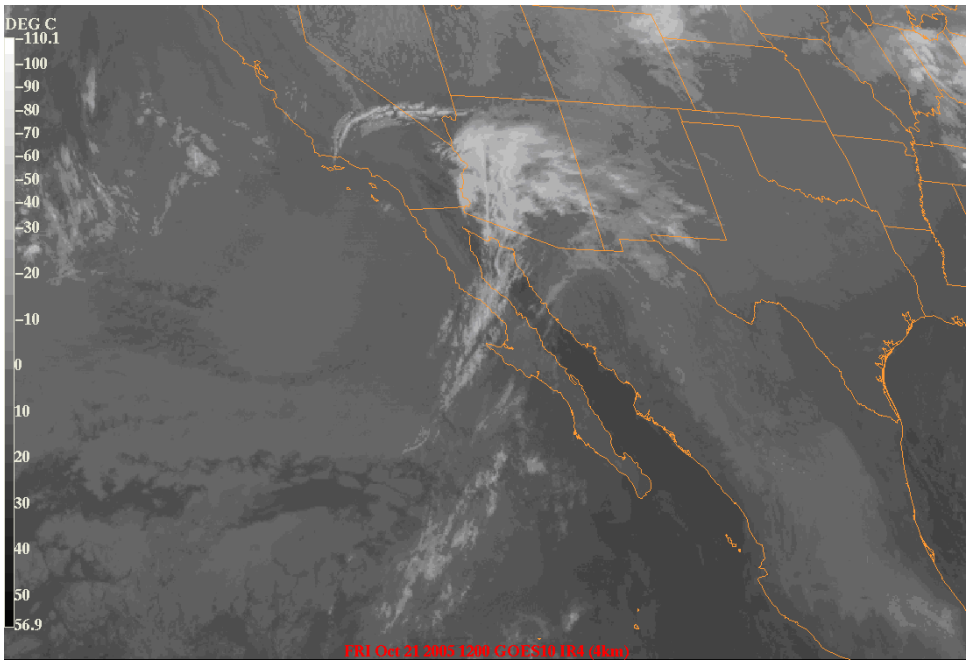

Figure 4.1.e. GOES-W image for valid at 21 Oct 05/12Z.

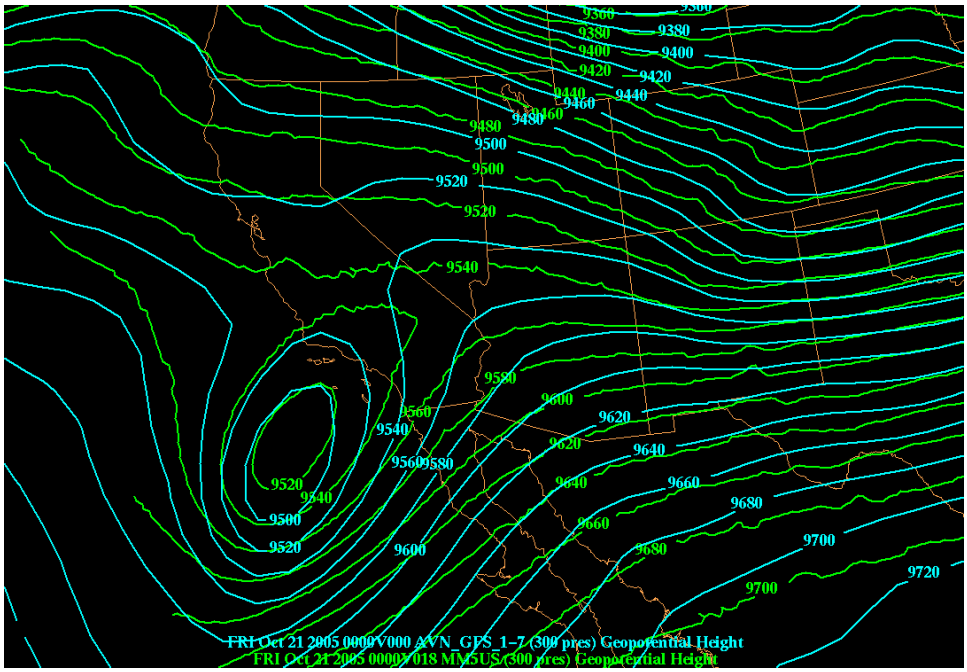

Figure 4.2.a. Verification of the 18-hour MM5 300mb height forecast (green contours) against the corresponding GFS analysis (blue contours) for 00Z on 21 Oct 05.

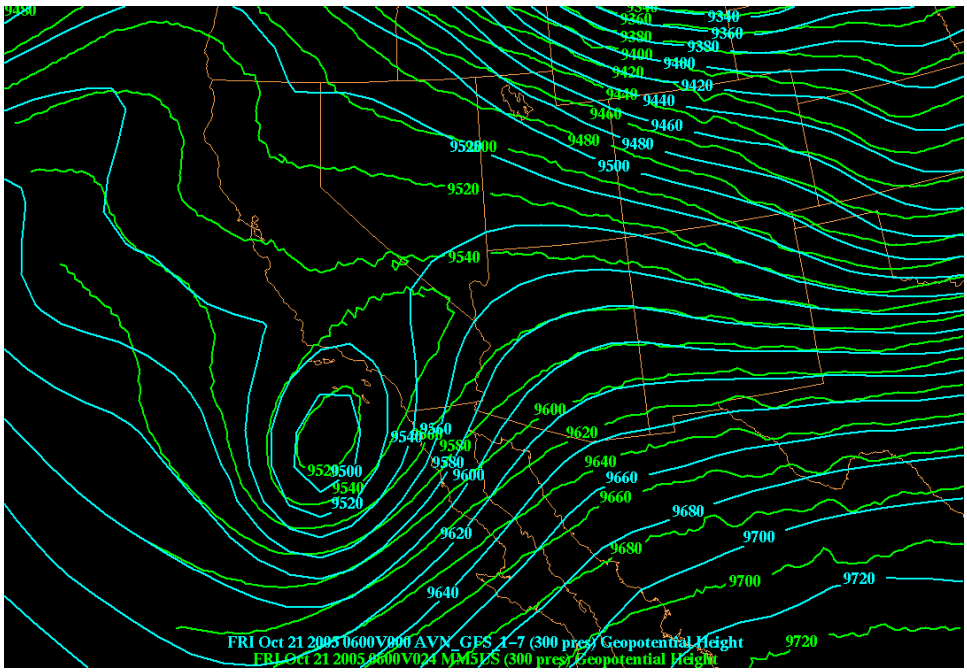

Figure 4.2.b. Verification of the 24-hour MM5 300mb height forecast (green contours) against the corresponding GFS analysis (blue contours) for 06Z on 21 Oct 05.

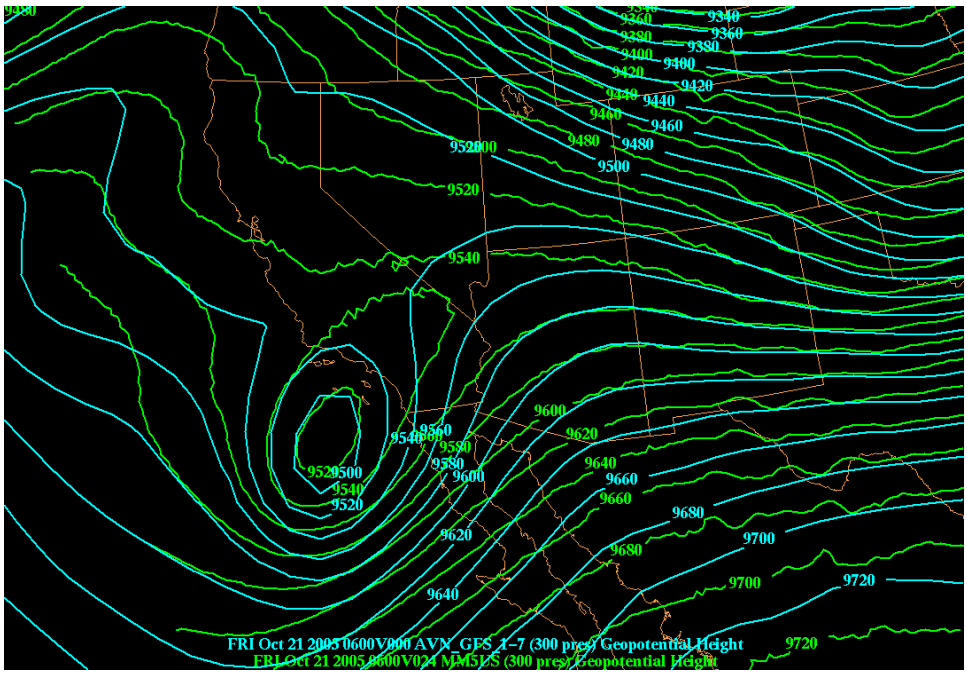

Figure 4.2.c. Verification of the 30-hour MM5 300mb height forecast (green contours) against the corresponding GFS analysis (blue contours) for 12Z on 21 Oct 05.

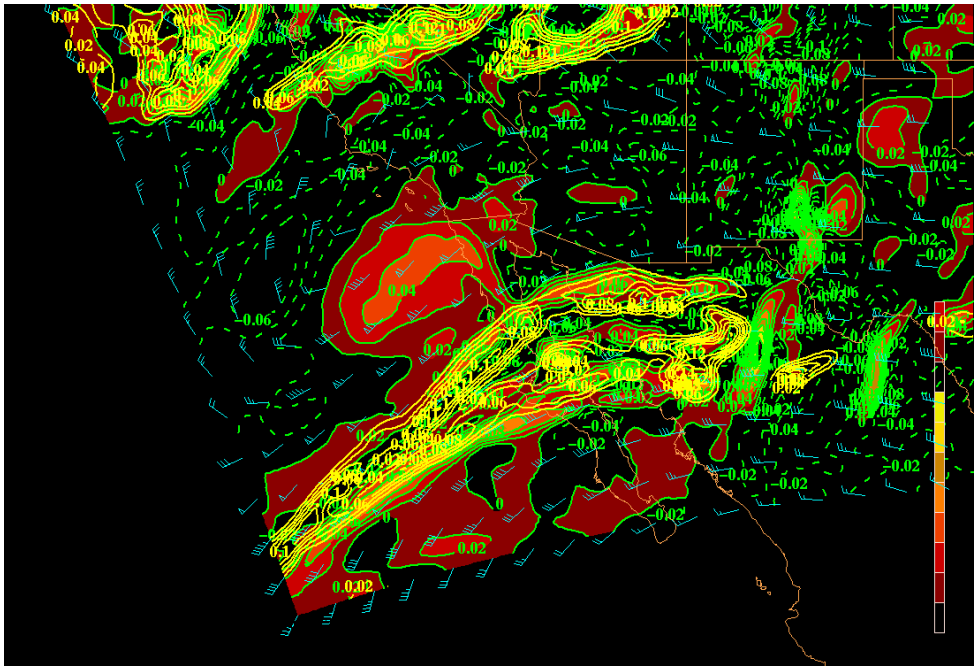

Figure 4.3.a. 300mb vertical motion and 2880 sigma ice water mixing ratio for 21/00Z. Ice water mixing ratio is in grams per kilogram x 10^{-2}, and upward vertical motion (represented by warm shades) is in m s^{-1}.

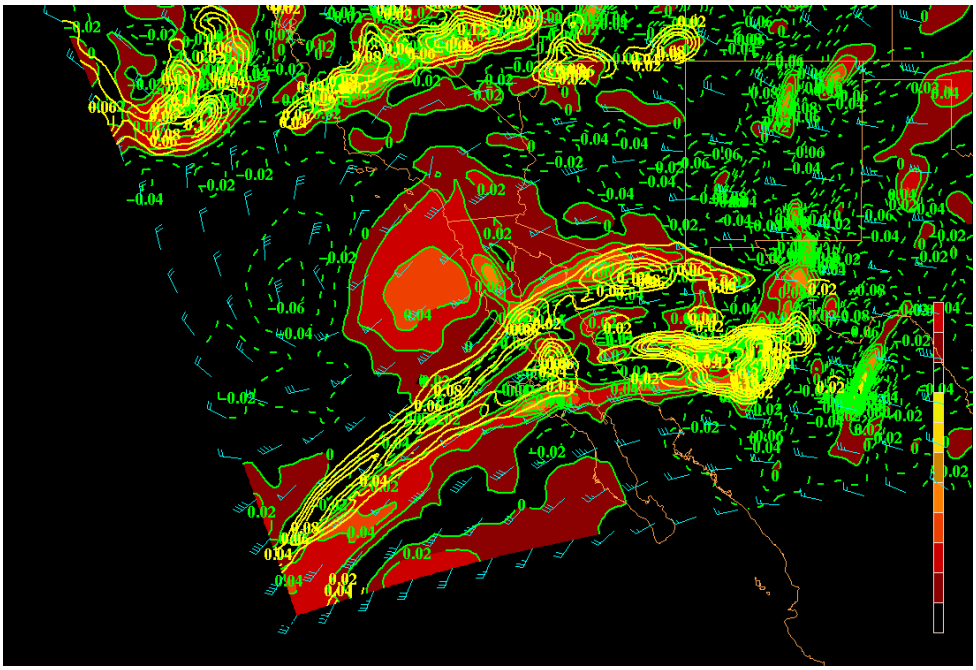

Figure 4.3.b. 300mb vertical motion and 2880 sigma ice water mixing ratio for 21/03Z. Ice water mixing ratio is in grams per kilogram x 10^{-2}, and upward vertical motion (represented by warm shades) is in m s^{-1}.

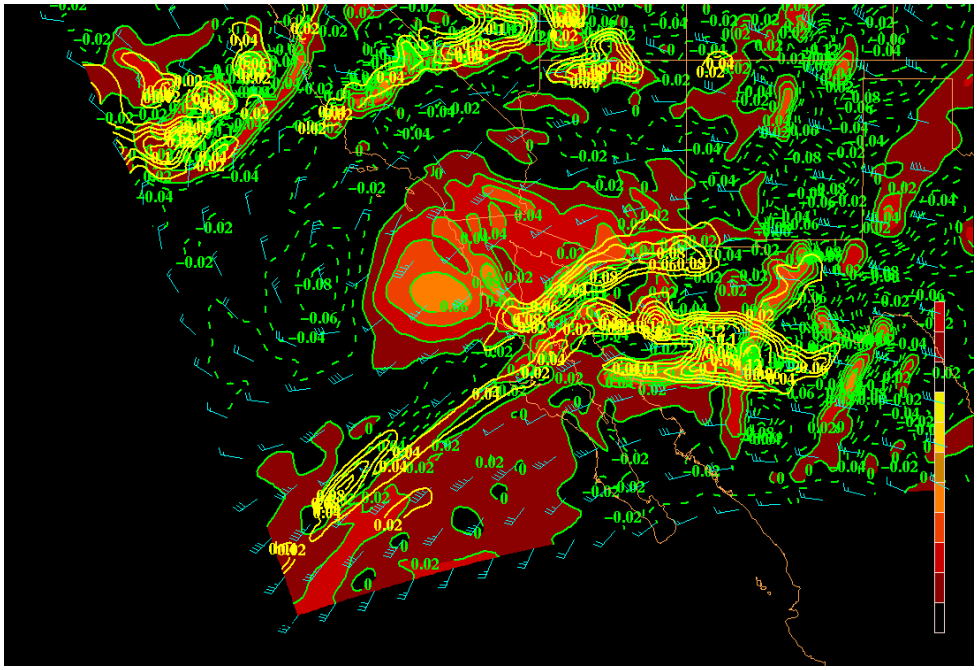

Figure 4.3.c. 300mb vertical motion and 2880 sigma ice water mixing ratio for 21/06Z. Ice water mixing ratio is in grams per kilogram x 10^{-2}, and upward vertical motion (represented by warm shades) is in m s^{-1}.

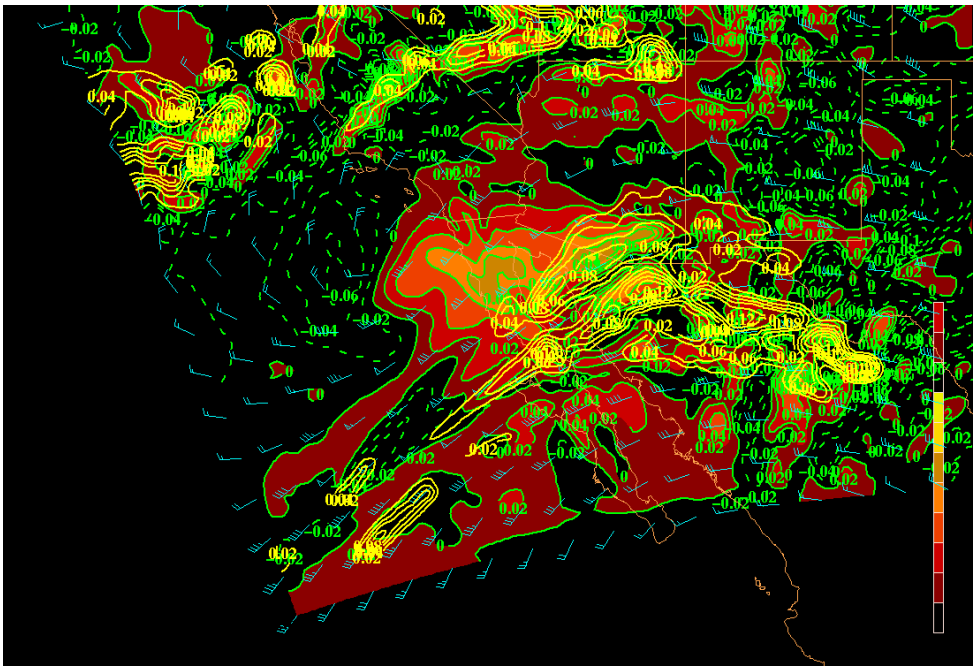

Figure 4.3.d. 300mb vertical motion and 2880 sigma ice water mixing ratio for 21/09Z. Ice water mixing ratio is in grams per kilogram x 10^{-2}, and upward vertical motion (represented by warm shades) is in m s^{-1}.

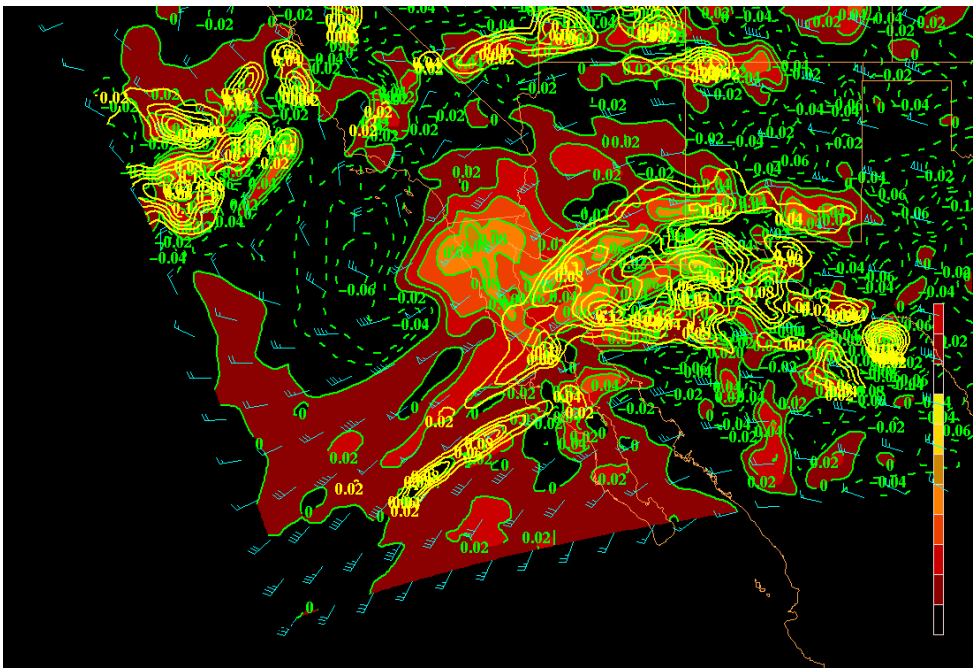

Figure 4.3.e. 300mb vertical motion and 2880 sigma ice water mixing ratio for 21/12Z. Ice water mixing ratio is in grams per kilogram x 10^{-2}, and upward vertical motion (represented by warm shades) is in m s^{-1}.

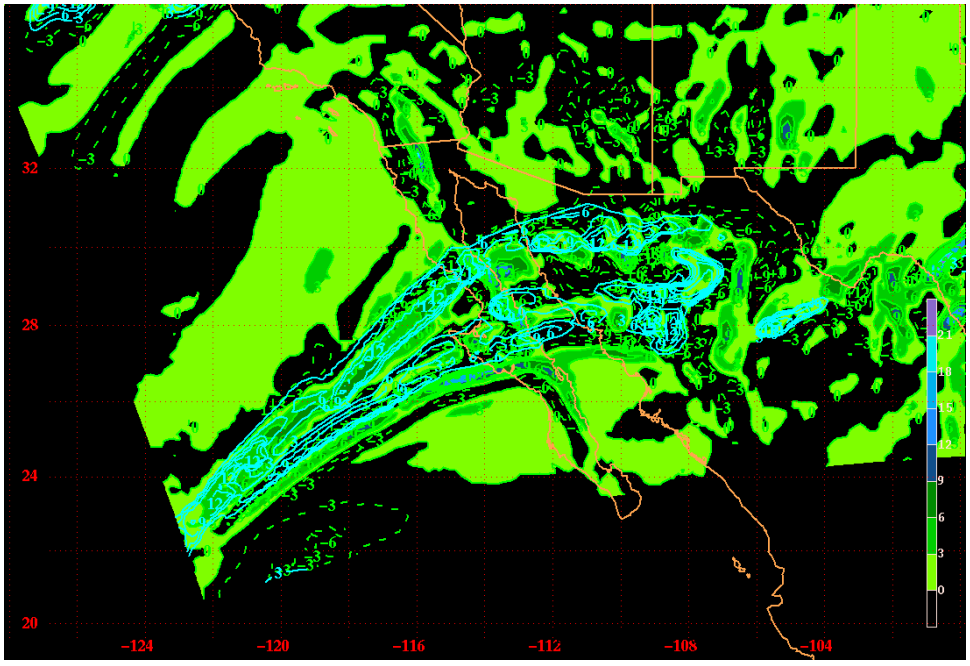

Figure 4.4.a. 2880 sigma ice water mixing ratio and moisture divergence for 21/00Z. Ice water mixing ratio is in grams per kilogram and areas of moisture divergence are shaded.

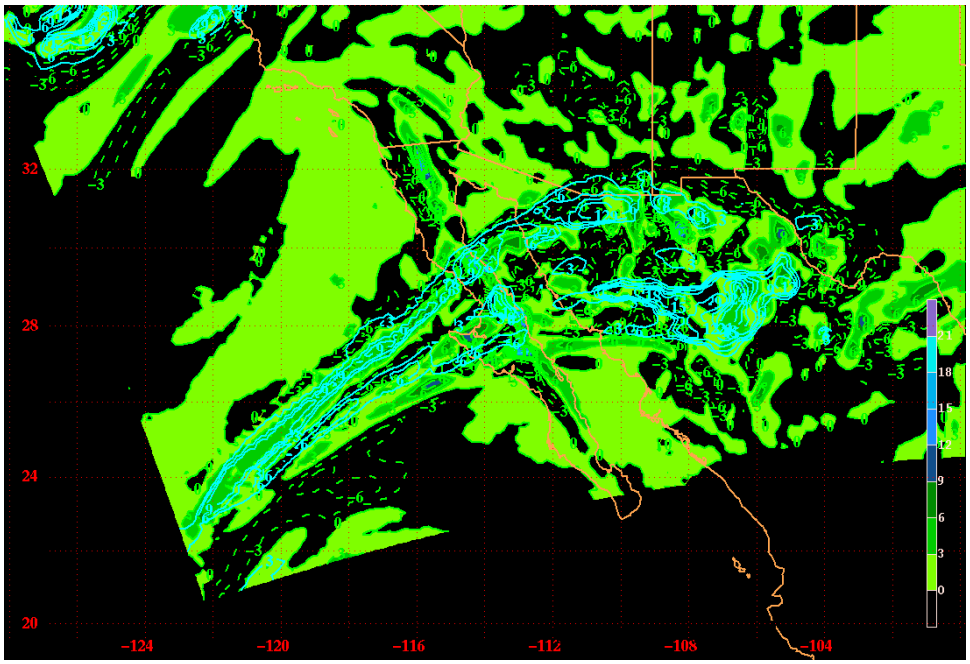

Figure 4.4.b. 2880 sigma ice water mixing ratio and moisture divergence for 21/03Z. Ice water mixing ratio is in grams per kilogram and areas of moisture divergence are shaded.

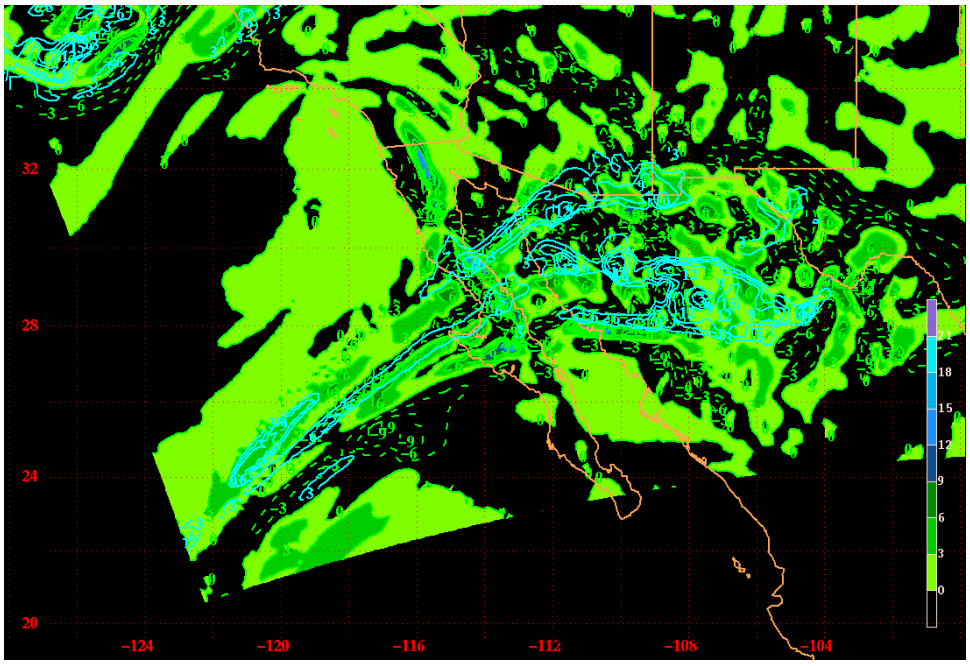

Figure 4.4.c. 2880 sigma ice water mixing ratio and moisture divergence for 21/06Z. Ice water mixing ratio is in grams per kilogram and areas of moisture divergence are shaded.

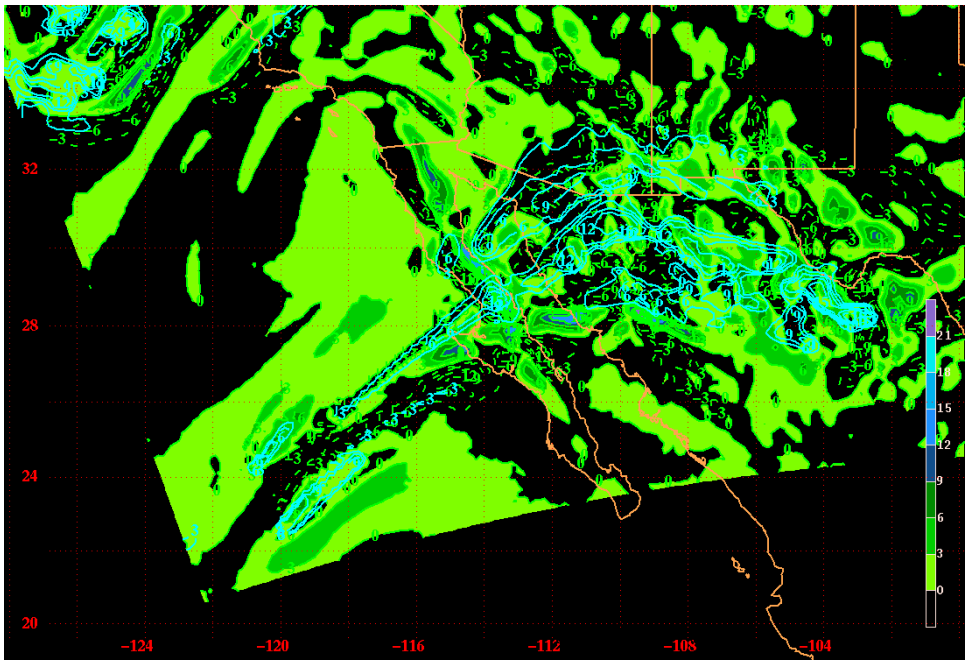

Figure 4.4.d. 2880 sigma ice water mixing ratio and moisture divergence for 21/09Z. Ice water mixing ratio is in grams per kilogram and areas of moisture divergence are shaded.

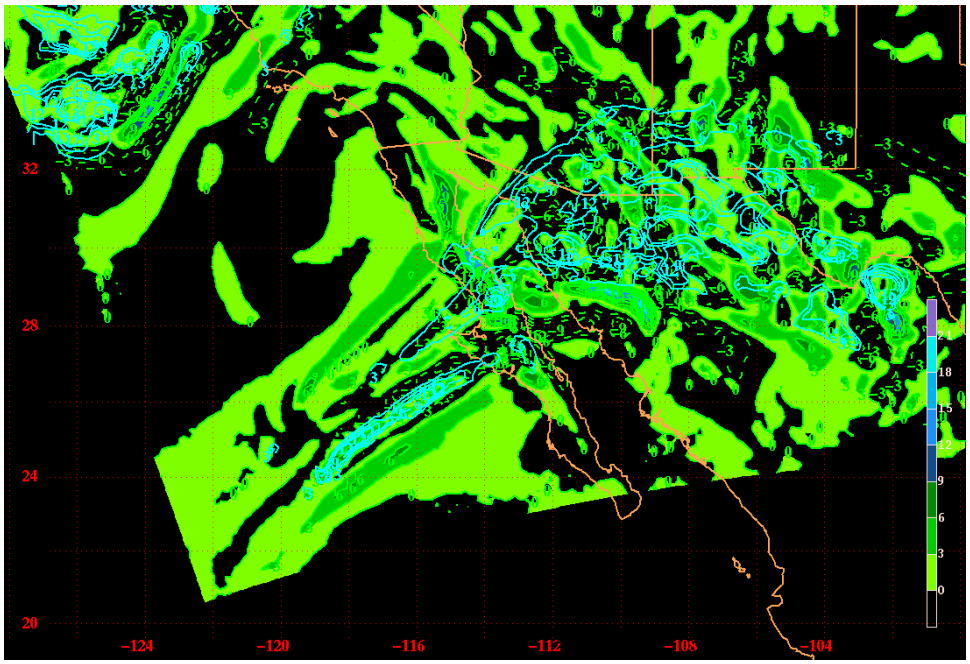

Figure 4.4.e. 2880 sigma ice water mixing ratio and moisture divergence for 21/12Z. Ice water mixing ratio is in grams per kilogram and areas of moisture divergence are shaded.

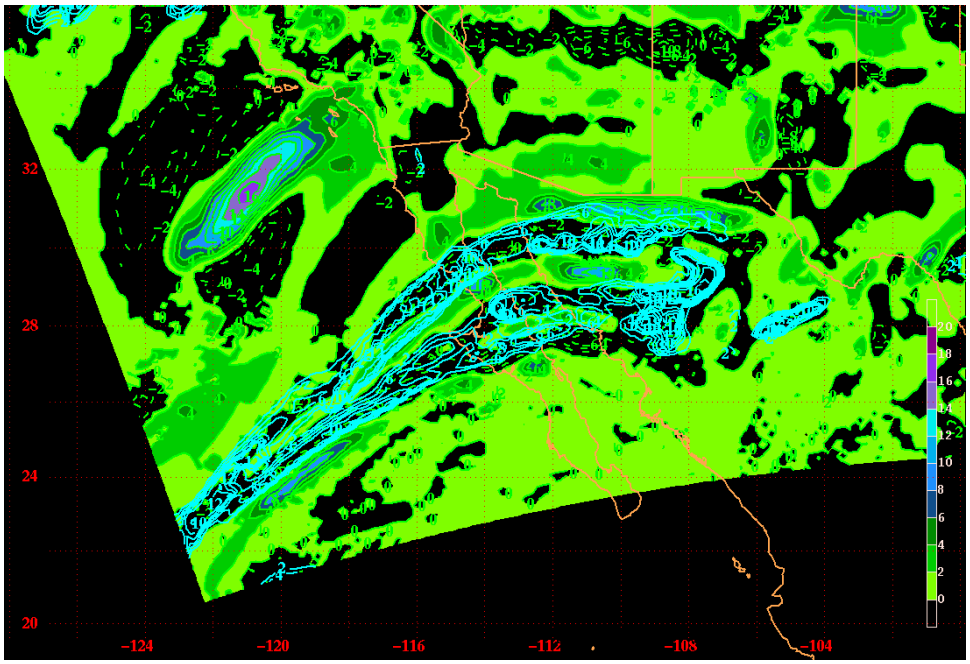

Figure 4.5.a. 2880 sigma ice water mixing ratio and frontogenesis for 21/00Z. Ice water mixing ratio is in grams per kilogram, and frontogenesis is represented by shaded areas.

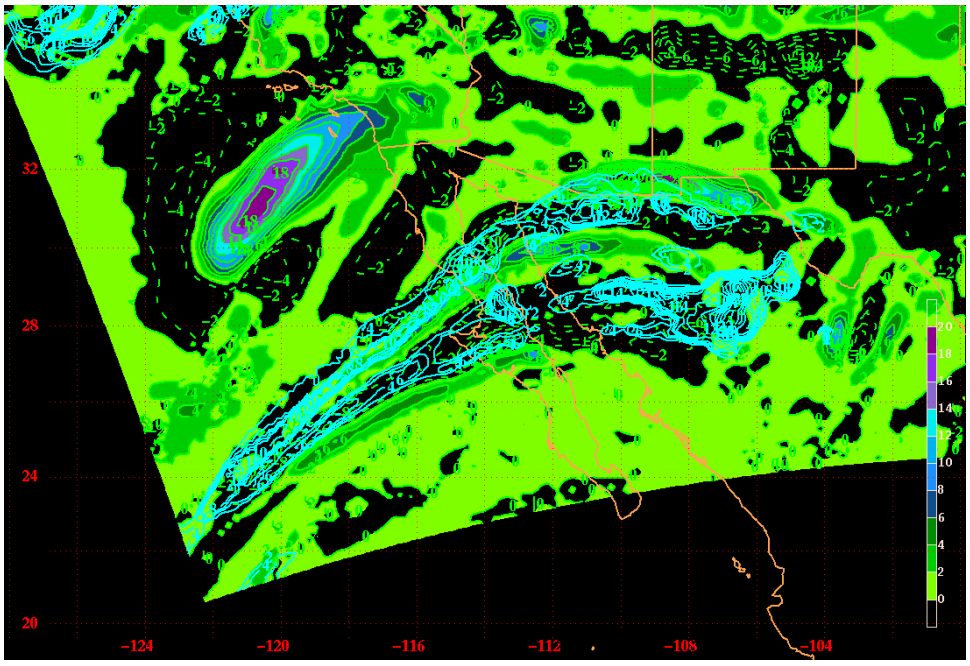

Figure 4.5.b. 2880 sigma ice water mixing ratio and frontogenesis for 21/03Z. Ice water mixing ratio is in grams per kilogram, and frontogenesis is represented by shaded areas.

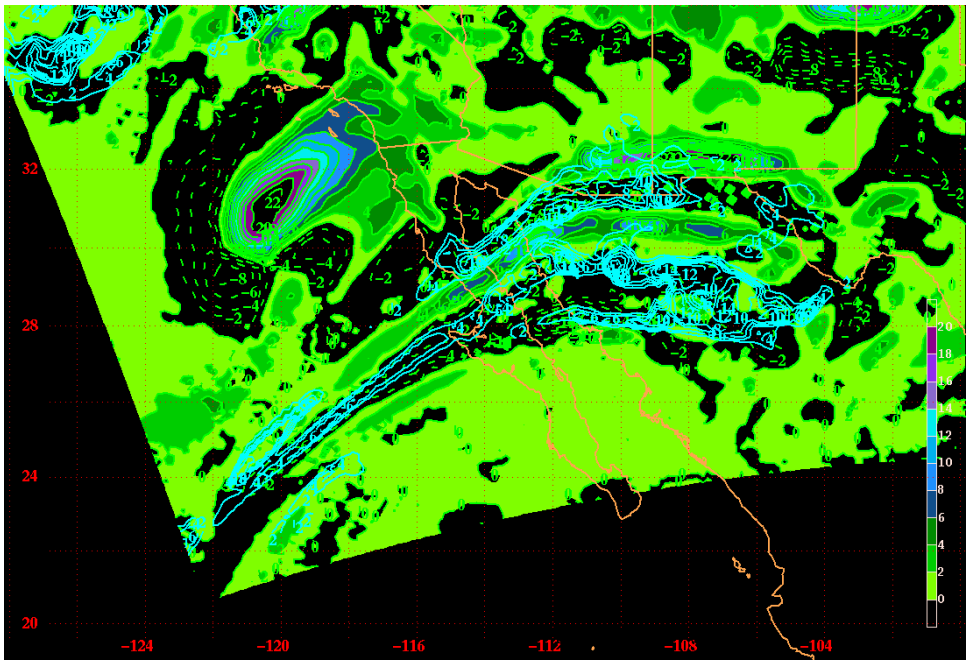

Figure 4.5.c. 2880 sigma ice water mixing ratio and frontogenesis for 21/06Z. Ice water mixing ratio is in grams per kilogram, and frontogenesis is represented by shaded areas.

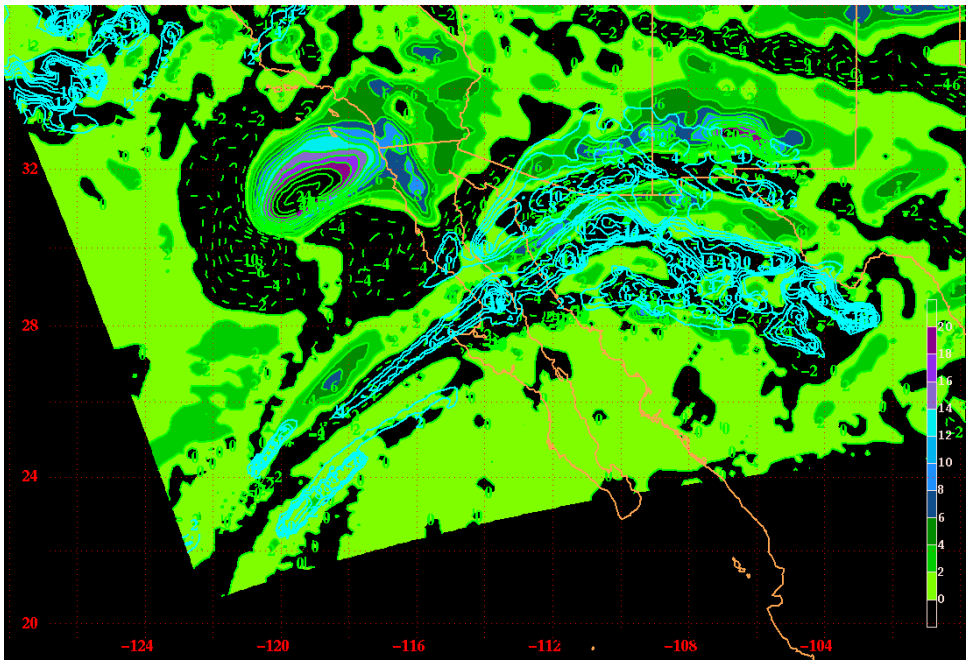

Figure 4.5.d. 2880 sigma ice water mixing ratio and frontogenesis for 21/09Z. Ice water mixing ratio is in grams per kilogram, and frontogenesis is represented by shaded areas.

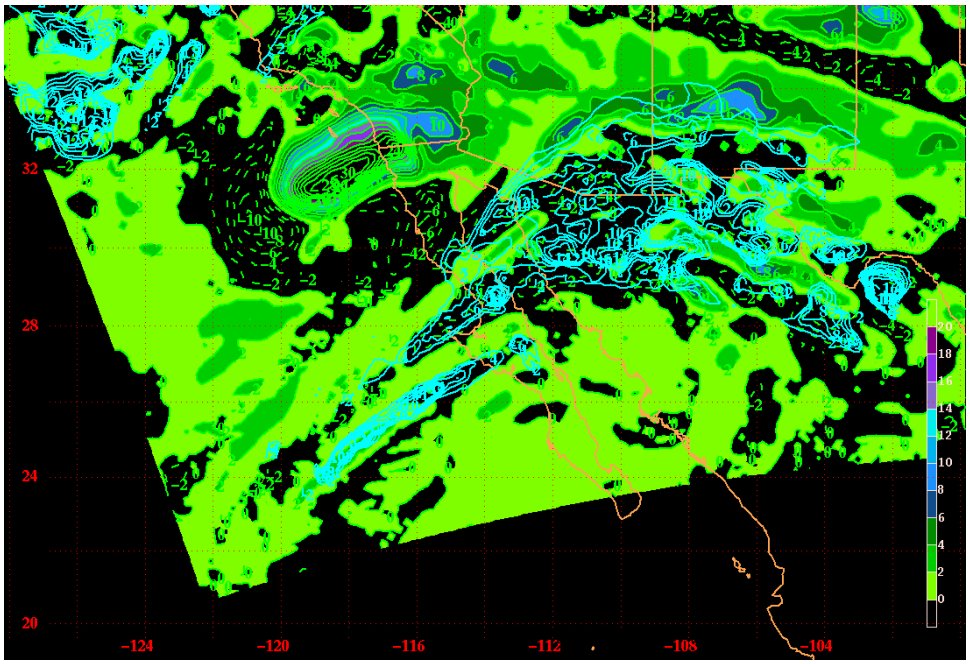

Figure 4.5.e. 2880 sigma ice water mixing ratio and frontogenesis for 21/12Z. Ice water mixing ratio is in grams per kilogram, and frontogenesis is represented by shaded areas.

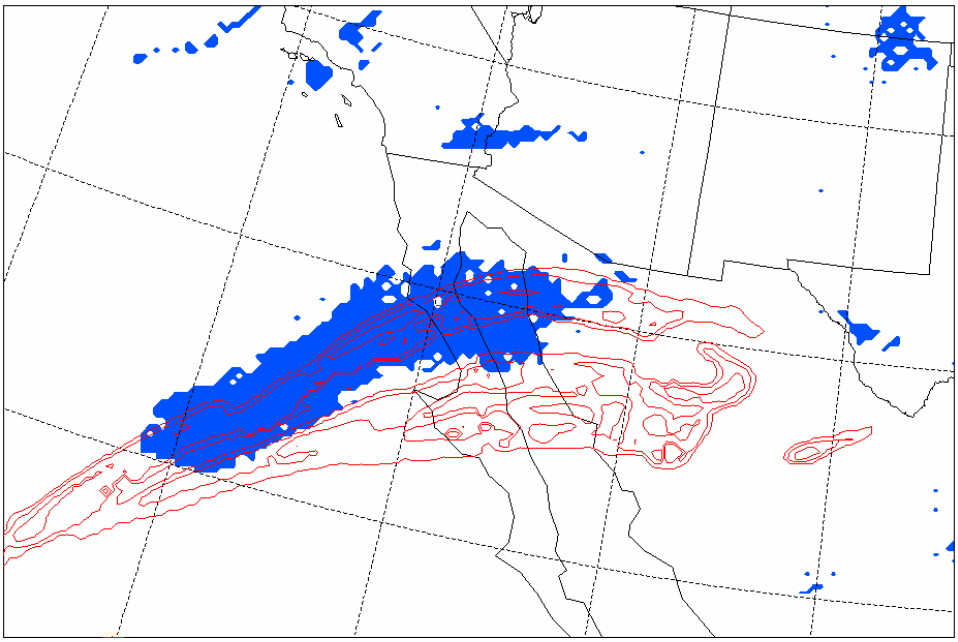

Figure 4.6.a. Composite ice water mixing ratio field vs cloud mask result for 21/00Z. Ice water mixing ratio returns are contoured, and ice cloud results from the cloud mask are in blue.

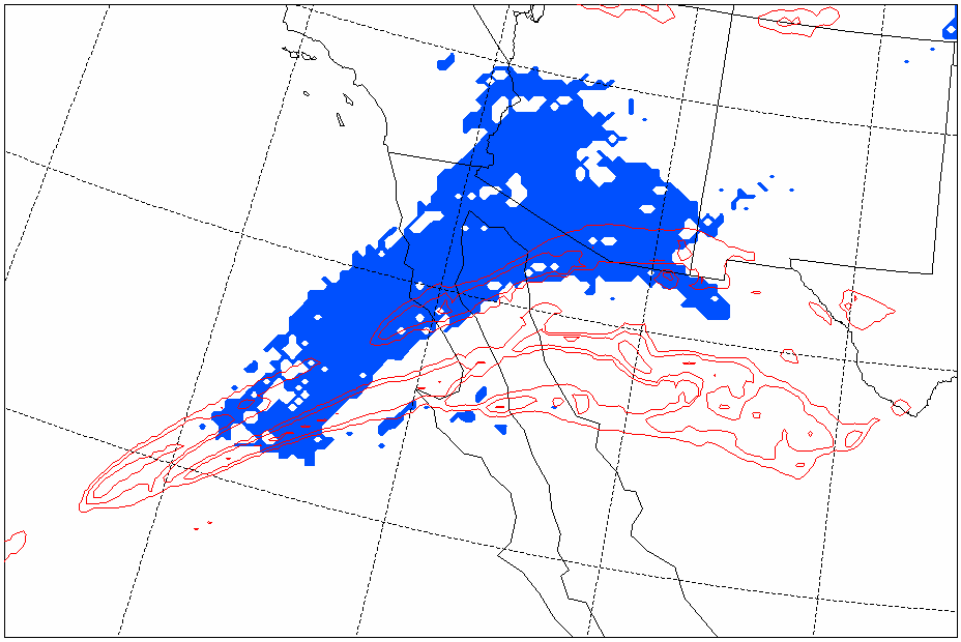

Figure 4.6.b. Composite ice water mixing ratio field vs cloud mask result for 21/06Z. Ice water mixing ratio returns are contoured, and ice cloud results from the cloud mask are in blue.

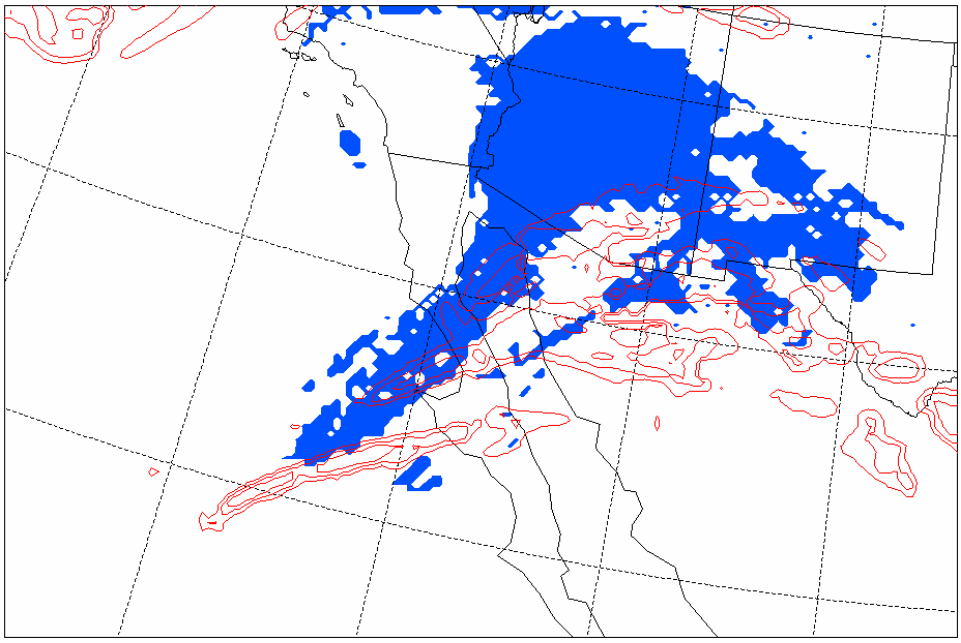

Figure 4.6.c. Composite ice water mixing ratio field vs cloud mask result for 21/12Z. Ice water mixing ratio returns are contoured, and ice cloud results from the cloud mask are in blue.

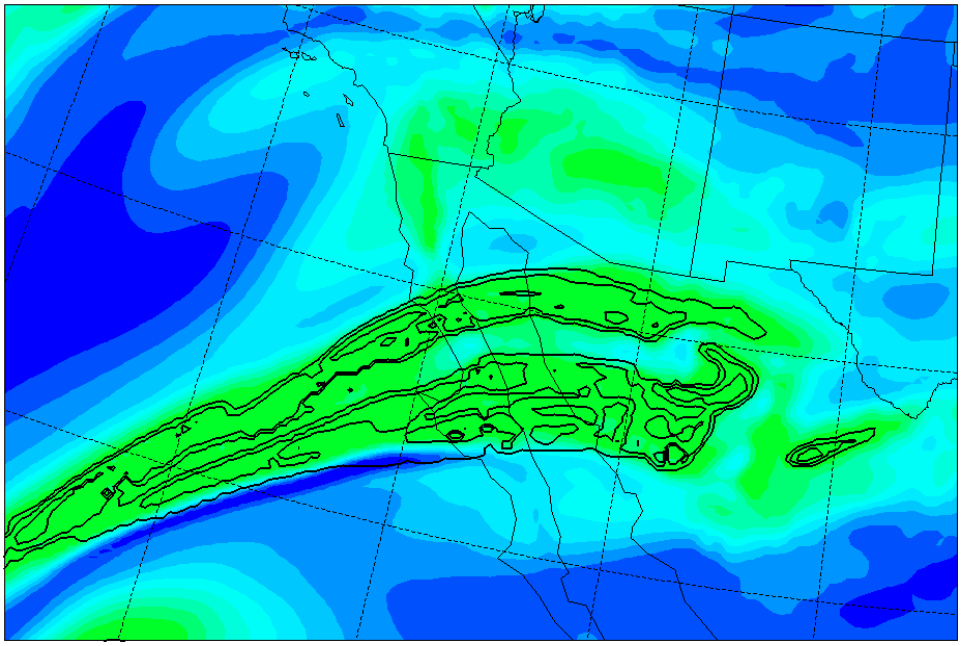

Figure 4.7.a. Relative humidity (with respect to ice) vs composite ice water mixing ratio for 21/00Z. Green shades indicate relative humidity of 90% and greater.

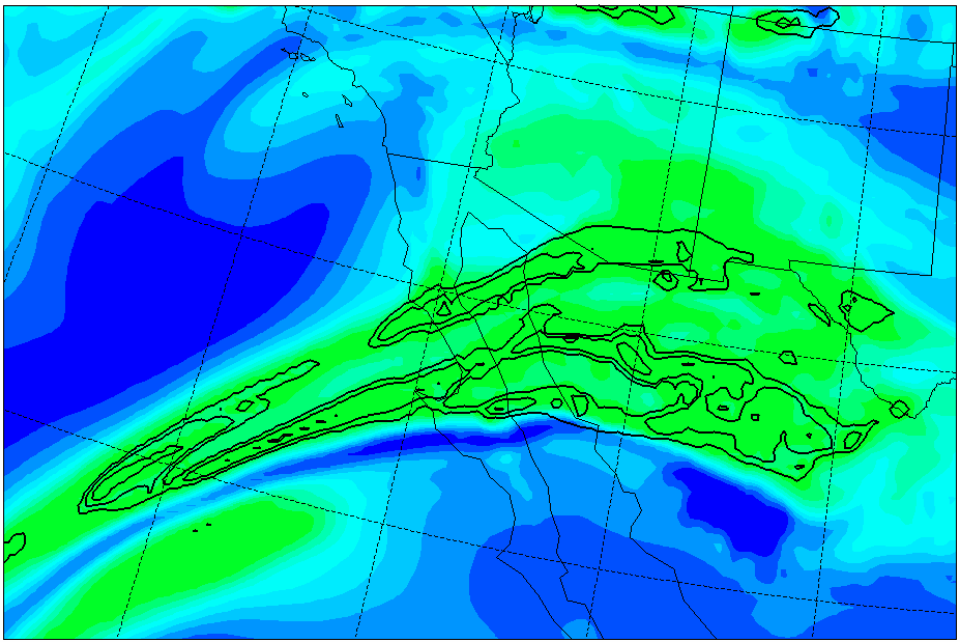

Figure 4.7.b. Relative humidity with (respect to ice) vs composite ice water mixing ratio for 21/06Z. Green shades indicate relative humidity of 90% and greater.

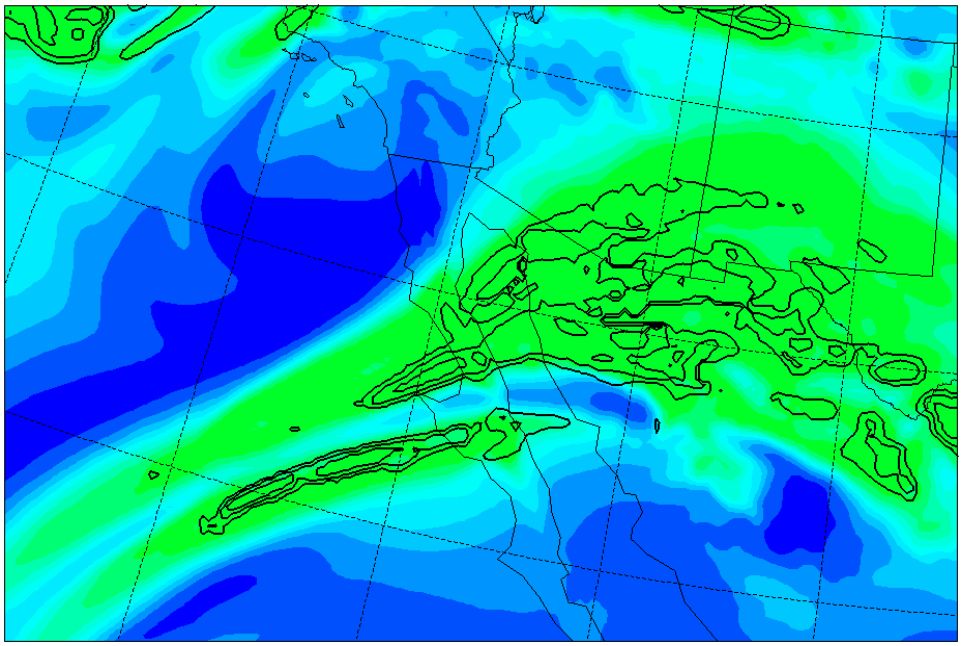

Figure 4.7.c. Relative humidity (with respect to ice) vs composite ice water mixing ratio for 21/12Z. Green shades indicate relative humidity of 90% and greater.

V. CASE STUDY II: UPPER-LEVEL RIDGE OVER ROCKIES

A. CASE DESCRIPTION

Case II involved cirrus associated with an upper-level trough/ridge pattern over the Rocky Mountain States from 26 Oct 05/00Z through 26 Oct 05/12Z. Figures 5.1.a through 5.1.e show the GOES infrared satellite images every three hours during the case study valid time. At 26/00Z, the main areas of interest were an elongated band of cirrus, which diminishes with time, located across the northern and central plains states and a more loosely organized area of ice cloud located over Utah. The ice clouds over Utah were the result of lift around a decaying upper low located in southeastern Nevada just prior to case study start time, whereas the cirrus clouds over the plains states were the result of advection across a ridge axis of moisture originally lifted by the low. Due to the configuration of the data collection system at the time the data were obtained for this case, 21-hour sigma data are not available for this case study.

B. MM5 FORECAST VERIFICATION

The 300mb height field for the case study valid time is shown in Figures 5.2.a through 5.2.c. The placement and intensity of the trof at 300mb is very similar between the GFS analysis and the MM5 forecast at all times, but the analyzed versus forecast ridge positions and intensities show minor differences. GFS-analyzed winds (not shown) were 10 to 15 knots stronger downwind of the ridge axis between the U.S.-Canada border and the central plains. This difference in wind speed was present at all analyzed levels between 200mb and 500mb.

One important difference between the GFS analyses and the MM5 forecasts is that the GFS appears to indicate a shortwave trof progressing through the pattern to the east of our area of interest, with a corresponding change in alignment of the height contours and resulting geostrophic winds. This results in a slightly more confluent area aloft over the northern and central plains, which may play a role in how the cirrus field in that area evolves during the forecast period.

C. ANALYSIS

Case Study I indicated that the presence of ice water in the model was tied strongly to upward vertical motion. This is valid in this case study as well, even in the area downstream of the ridge where production should not occur, as evident in comparisons of the upward motions shown in Figures 5.3.a, 5.3.c, and 5.3.e to the ice water field for corresponding times shown in Figures 5.4.a through 5.4.c. The vertical motion fields shown in Figures 5.3.a through 5.3.e indicate very weak, large-scale upward motion associated with the area downwind of the trof over Nevada and immediately east of the ridge axis. These upward motions are not very well organized, as evident in the pockets of upward and downward motions over eastern Colorado, Wyoming, and Montana in Figure 5.3.a. The upward motion field east of the ridge axis becomes more organized by 06Z (as seen in Figure 5.3.c) as a result of the trough lifting northeastward in the MM5 (Figure 5.2.b.) Stronger, better organized upward motion is located near the upper low over Utah throughout the case study period.

As mentioned earlier, this case provides two distinct areas of interest with regard to ice cloud coverage. For the first area, downstream of the ridge axis, the model's ice returns were located at higher altitudes—generally above 4145 sigma. Peak ice water mixing ratio values downstream of the ridge axis occur at 1460 sigma as shown in Figures 5.5.a through 5.5.d. Ice water mixing ratio results indicate diminishing ice water coverage within this plume as time progresses, and agree well with observed cirrus location. The second distinct area of ice cloud coverage was closer to the upper-level low, upstream of the ridge axis. Here, the most extensive ice water coverage ahead of the low is concentrated between the 4145 and 6065 sigma levels, with some traces of ice remaining at lower levels. In this location ice water returns are not as consistent vertically as in the first case. Additionally, convective elements are present in the returns for this case as indicated by darker contoured areas resembling bullseyes in Figures 5.4.a through 5.4.c and 5.6.a through 5.6.c. The model overforecast ice water coverage in this area as evident in Figures 5.4.a through 5.4.c, particularly over Colorado, Wyoming, Idaho, and Utah. In these locations, abundant ice water was present in areas absent of observed clouds.

D. RESULTS

With regard to basic forecast error, the second case posed somewhat less of a challenge for the MM5 than the first case. Figures 4.2.a through 4.2.c show significant phase error in the model versus observed conditions, whereas Figures 5.2.a through 5.2.c show the model handled evolution of the synoptic situation fairly well. Discrepancies did arise in the position of the downstream ice cloud in Figures 5.4.a through 5.4.c, indicating the presence of a slight timing error. Additionally, along this downstream plume, coverage of ice was more continuous in the model than indicated in the cloud mask. Near the low, significant differences arose in the placement of ice cloud. The model appeared to tie ice cloud very strongly to upward motions, so the presence of sufficient moisture and upward motion appeared to result in an overforecast of ice cloud in this location. Comparison of the ice water field to the cloud mask, shown in Figure 5.4.a, shows that ice cloud over northern Arizona was slightly underforecast, although the model did a slightly more respectable job of forecasting ice cloud over Utah at this time. Significant overforecasting of ice cloud occurred over western Colorado, southwestern Wyoming and eastern Idaho, corresponding to areas of upward motion as shown in Figure 5.3.a. Figure 5.4.b shows significant error across Wyoming, and also some timing and coverage errors associated with the downstream plume across northeastern Colorado. By 26/12Z, the model did a very respectable job depicting ice water coverage over Colorado, but appeared to underforecast ice over northern New Mexico. This appears to be due to insufficient moisture in the area, as mixing ratio values across the area were initially very low and increase only slightly by 26/12Z.

The 90% relative humidity (with respect to ice) field shows nearly saturated air over Wyoming in Figure 5.6.a whereas the corresponding satellite image (shown in Figure 5.1.a) and cloud mask image (shown in Figure 5.4.a) show only a swath of high moisture over eastern Wyoming. The relative humidity field suggests that ample moisture to the northeast of the low, when coupled with vertical motion of sufficient strength, leads to the erroneous cloud cover over Colorado, Wyoming, and Utah mentioned above. The broad area of high relative humidity and loosely organized vertical motion lead to cirrus in areas that do not match the observed clouds in detail.

This represents a significant forecast challenge to get the vertical motion exactly right so that cirrus are not over predicted in this broad area of high relative humidity.

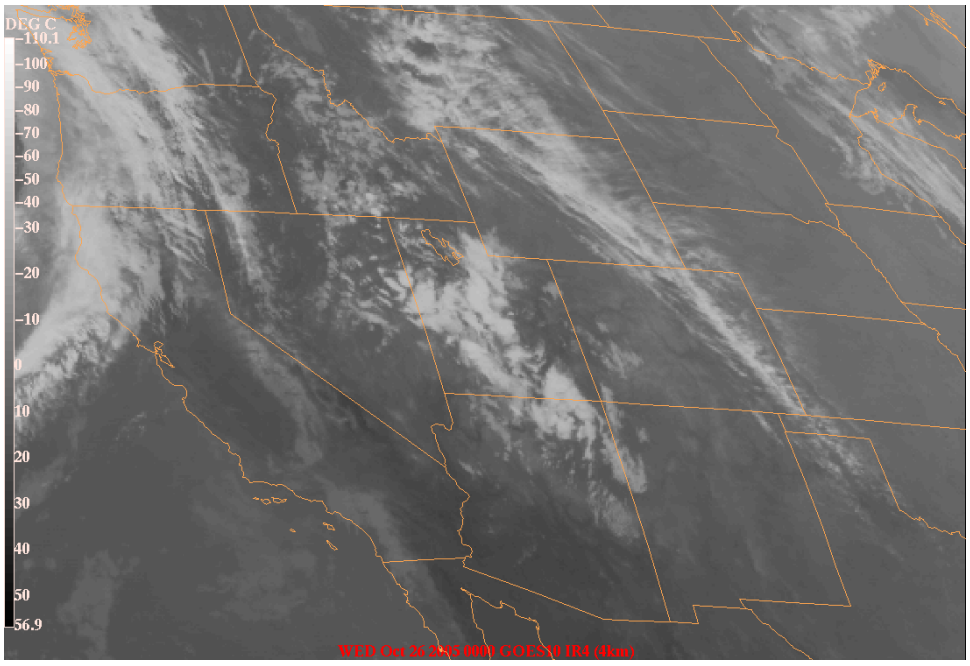

Figure 5.1.a. GOES-W image valid at 26 Oct 05/00Z.

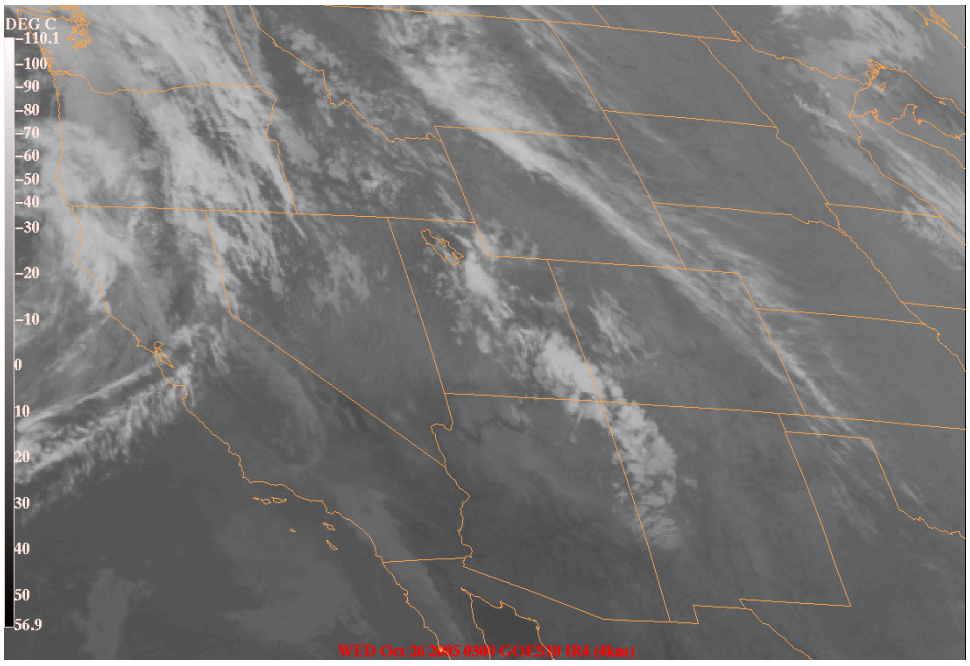

Figure 5.1.b. GOES-W image valid at 26 Oct 05/03Z.

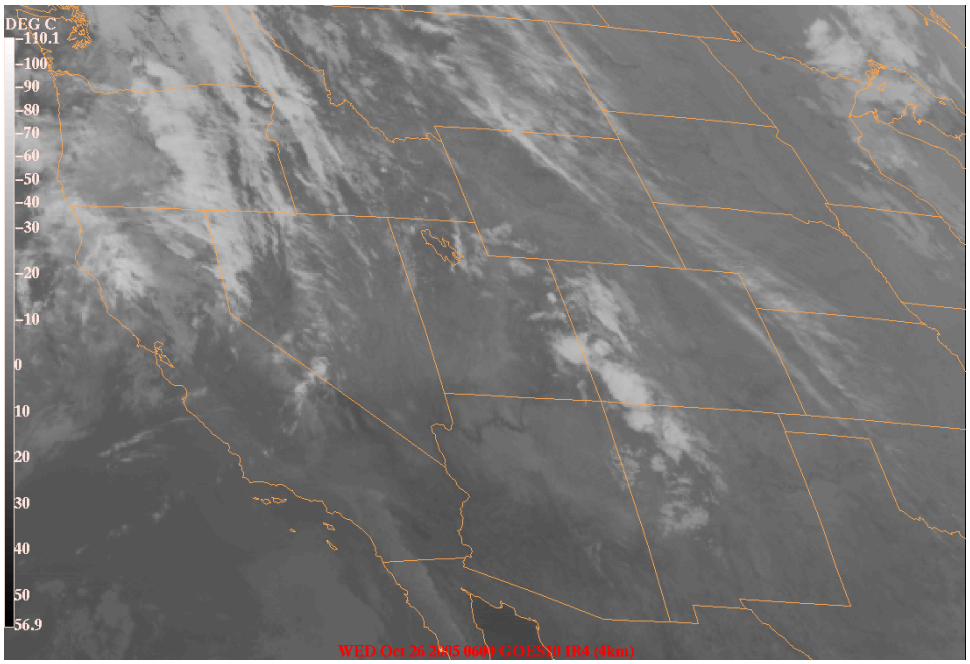

Figure 5.1.c. GOES-W image valid at 26 Oct 05/06Z.

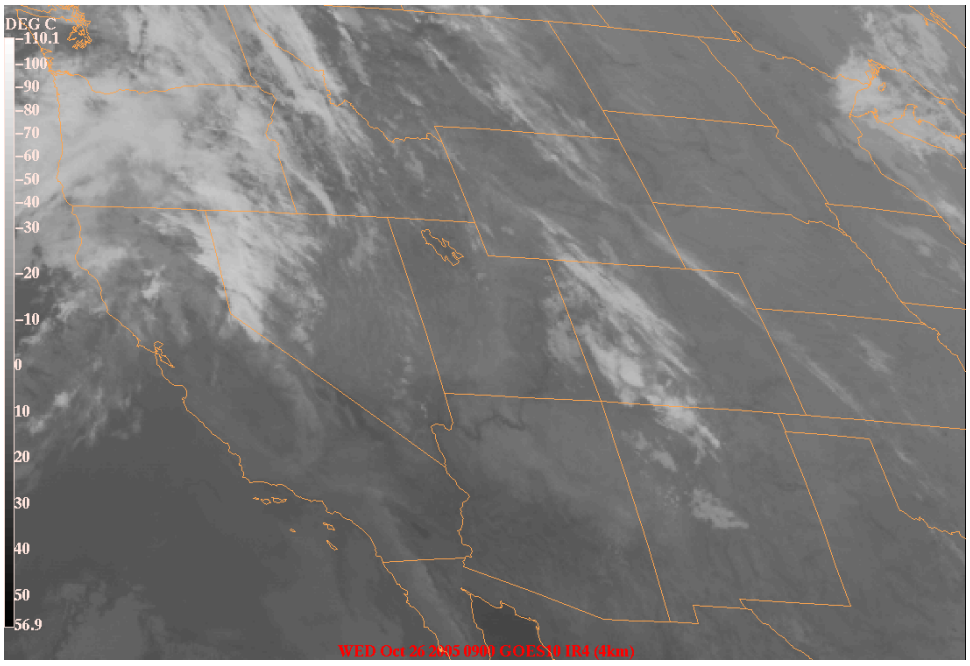

Figure 5.1.d. GOES-W image valid at 26 Oct 05/09Z.

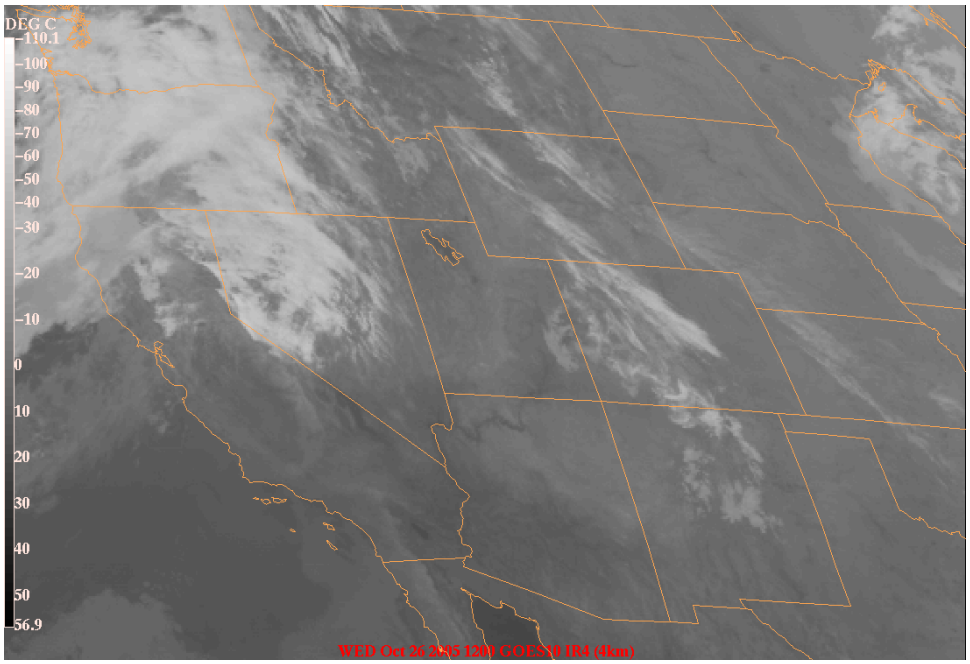

Figure 5.1.e. GOES-W image valid at 26 Oct 05/12Z.

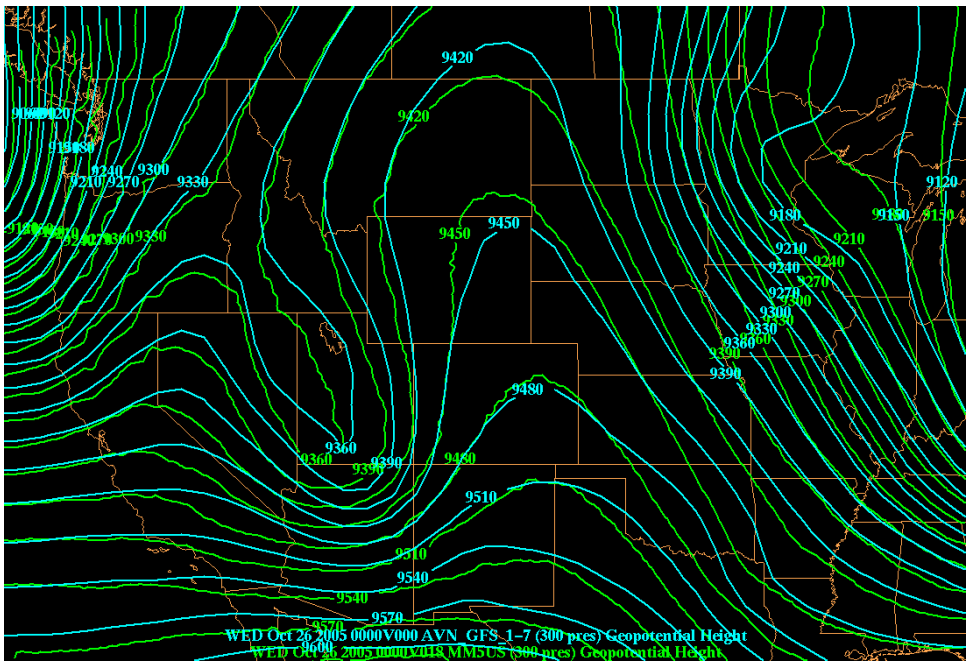

Figure 5.2.a. Verification of the 18-hour MM5 300mb height forecast (green contours) against the corresponding GFS analysis (blue contours) for 00Z on 26 Oct 05.

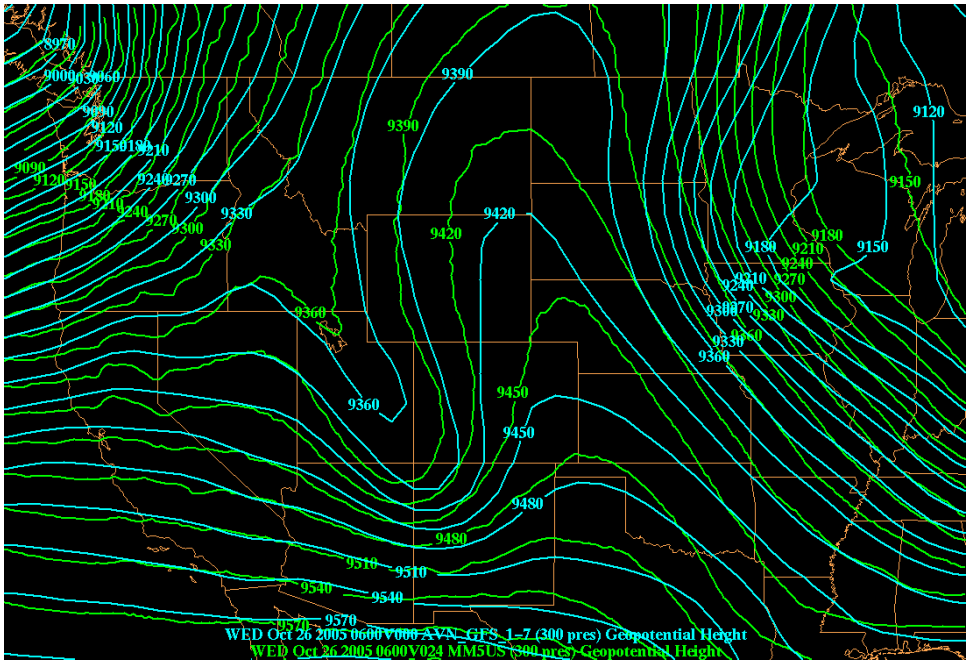

Figure 5.2.b. Verification of the 24-hour MM5 300mb height forecast (green contours) against the corresponding GFS analysis (blue contours) for 06Z on 26 Oct 05.

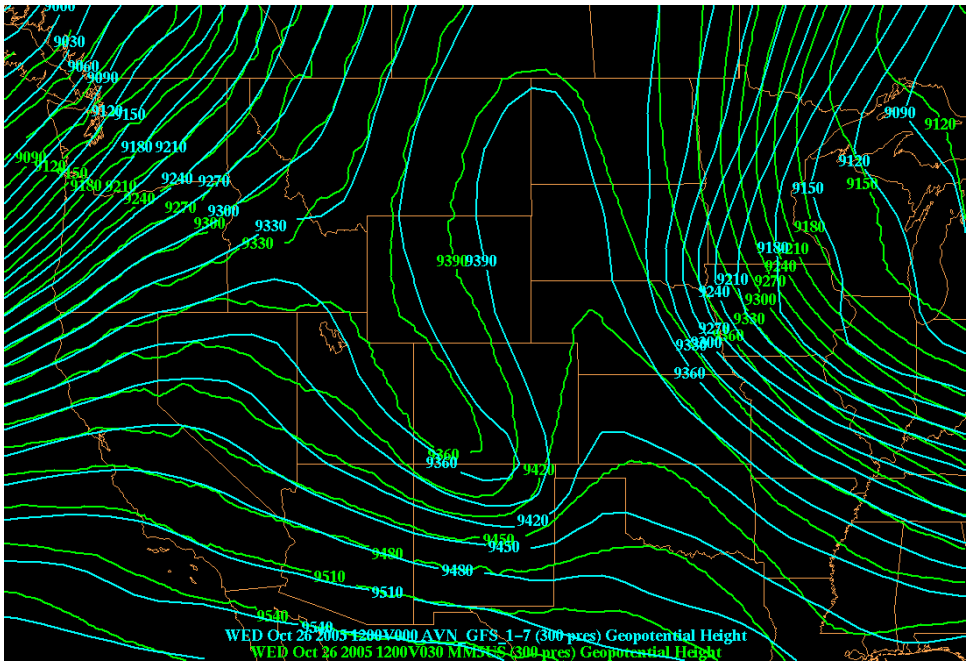

Figure 5.2.c. Verification of the 30-hour MM5 300mb height forecast (green contours) against the corresponding GFS analysis (blue contours) for 12Z on 26 Oct 05.

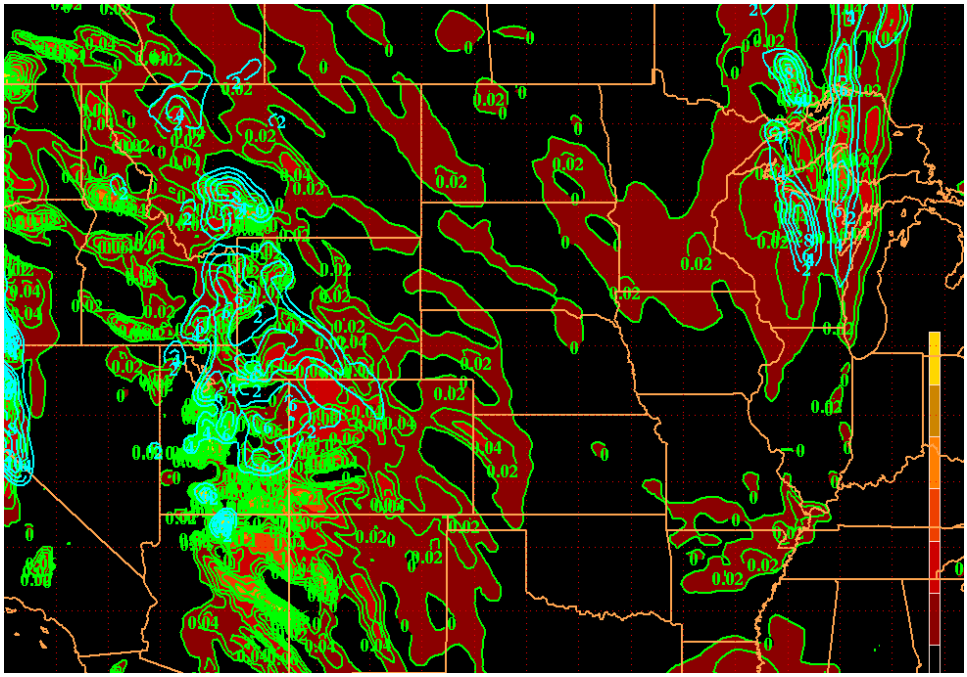

Figure 5.3.a. 400mb vertical motion and 4145 sigma ice water mixing ratio for 26/00Z. Upward vertical motion is represented by warm shades, and ice water mixing ratio is in blue contours.

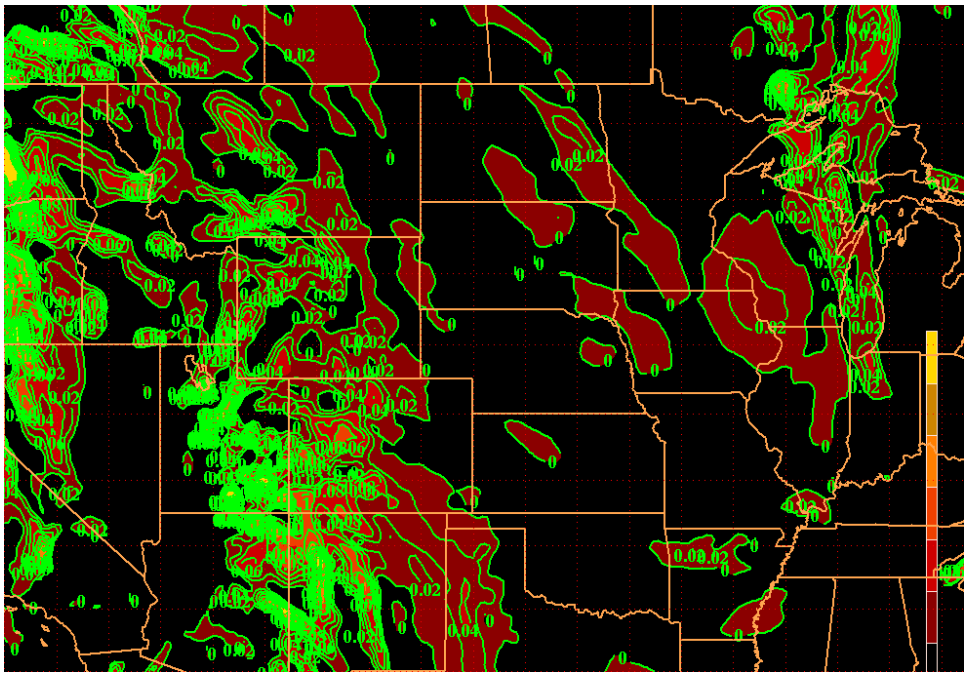

Figure 5.3.b. 400mb vertical motion at 26/03Z. Sigma level data were not available for this time; as a result, the ice water field is not available. Upward vertical motion is represented by warm shades.

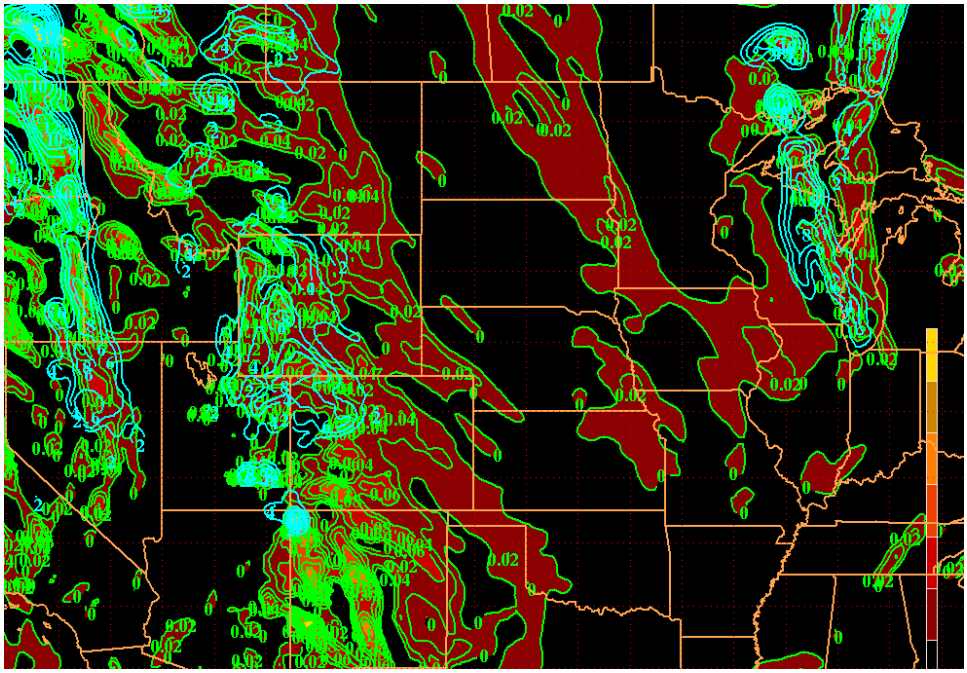

Figure 5.3.c. 400mb vertical motion and 4145 sigma ice water mixing ratio for 26/06Z. Upward vertical motion is represented by warm shades, and ice water mixing ratio is in blue contours.

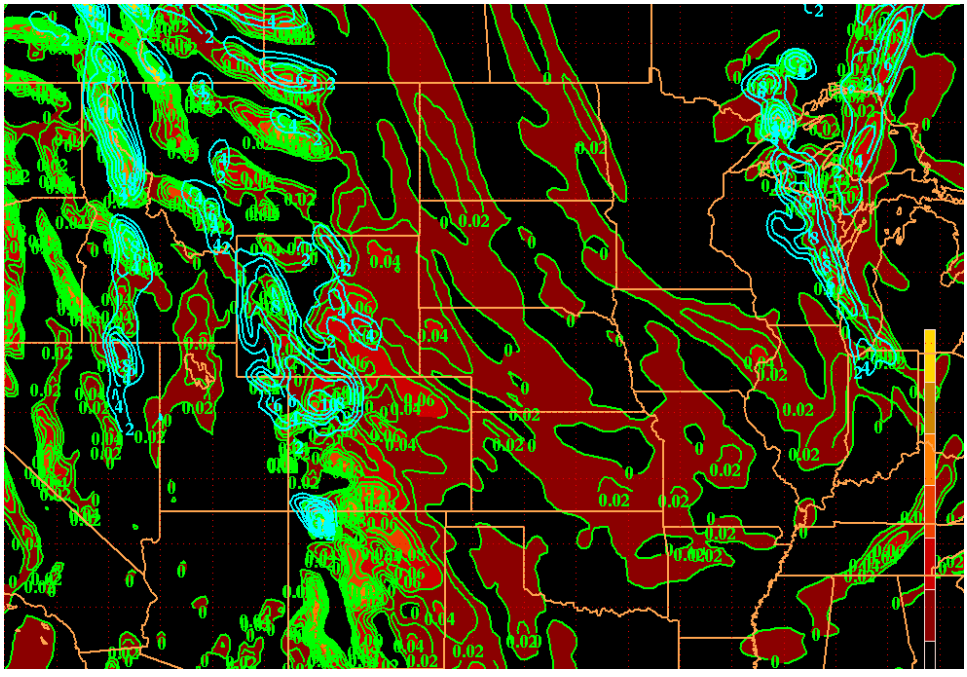

Figure 5.3.d. 400mb vertical motion and 4145 sigma ice water mixing ratio for 26/09Z. Upward vertical motion is represented by warm shades, and ice water mixing ratio is in blue contours.

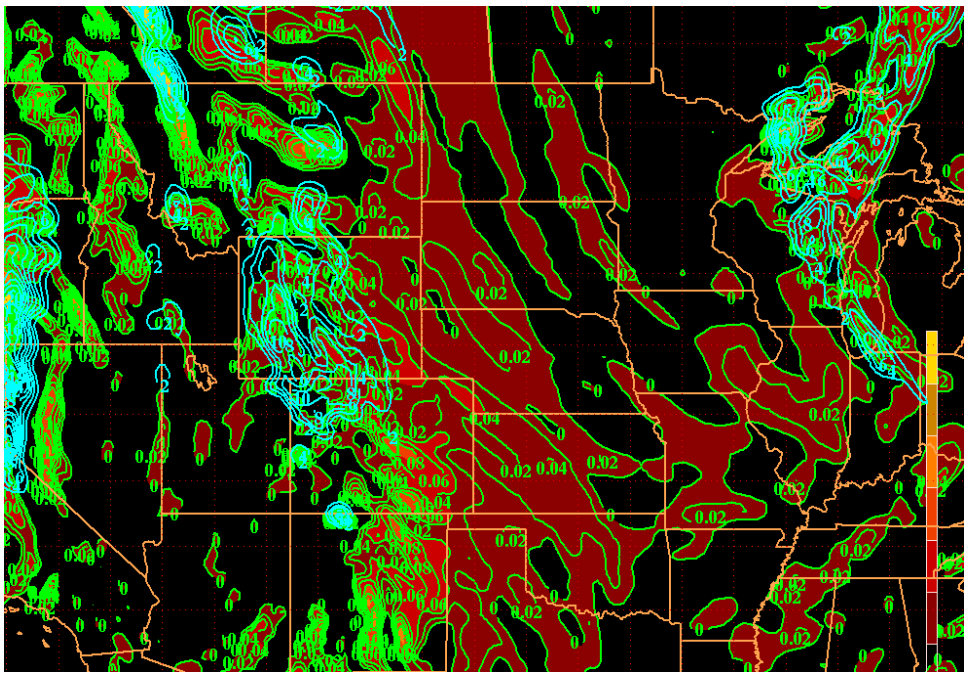

Figure 5.3.e. 400mb vertical motion and 4145 sigma ice water mixing ratio for 26/12Z. Upward vertical motion is represented by warm shades, and ice water mixing ratio is in blue contours.

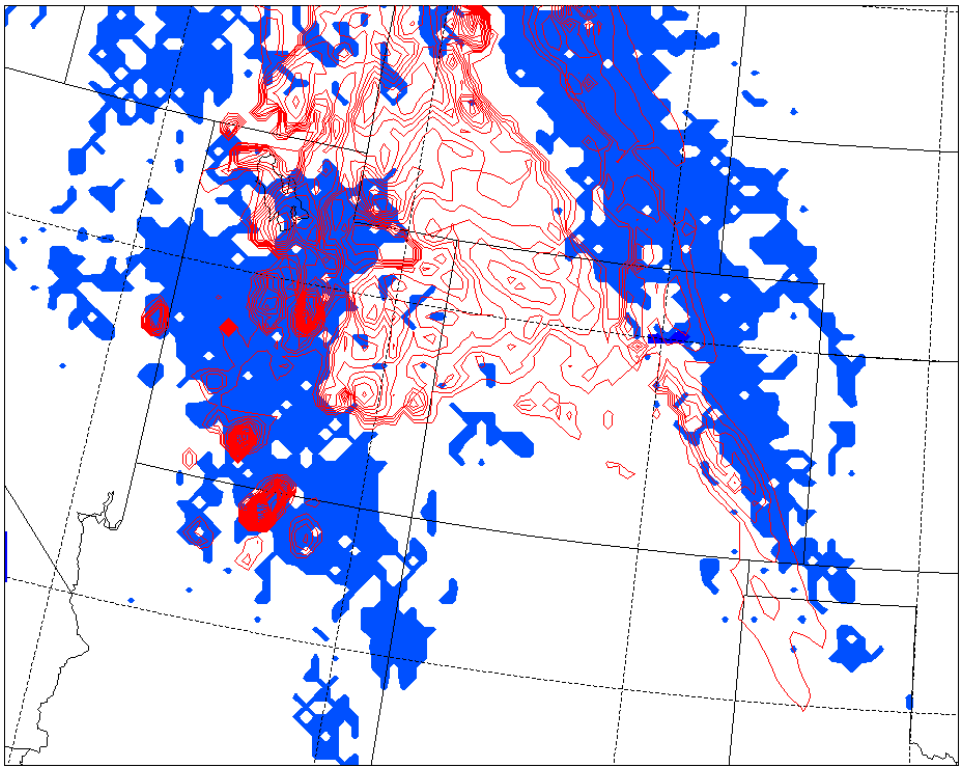

Figure 5.4.a. Composite ice water mixing ratio field vs cloud mask result for 26/00Z.

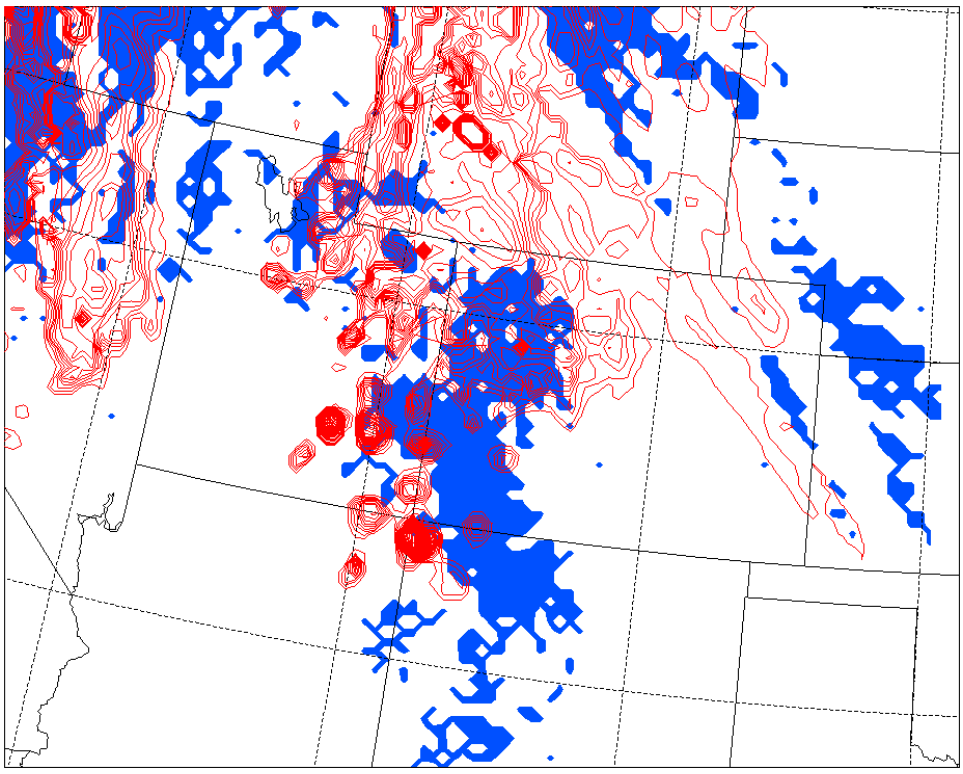

Figure 5.4.b. Composite ice water mixing ratio field vs cloud mask result for 26/06Z.

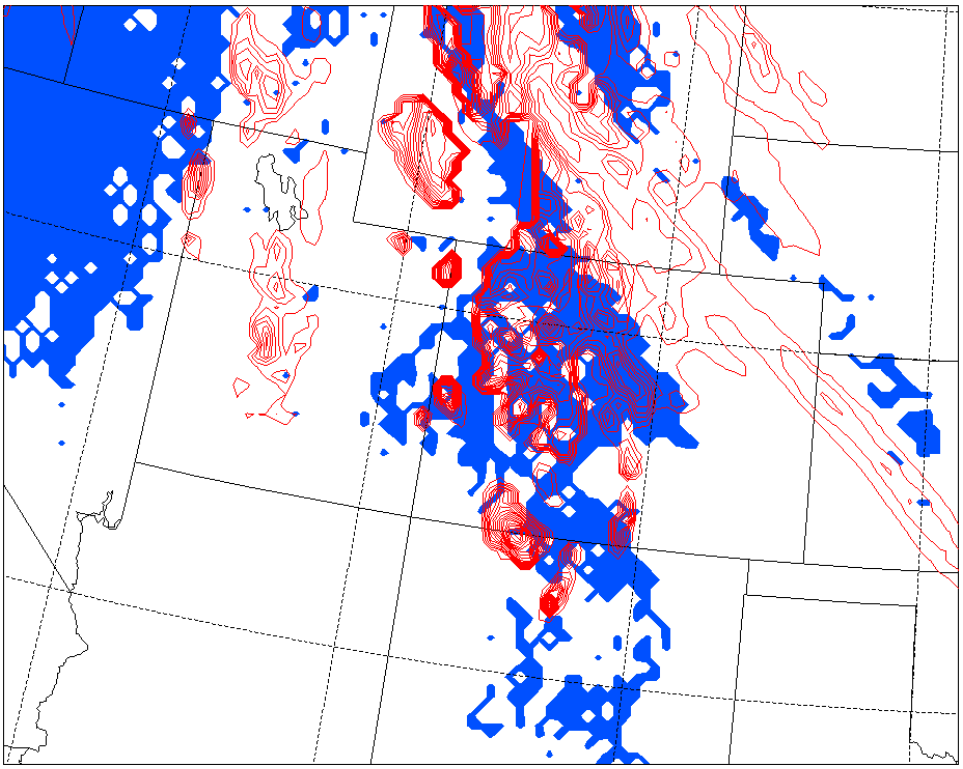

Figure 5.4.c. Composite ice water mixing ratio field vs cloud mask result for 26/12Z.

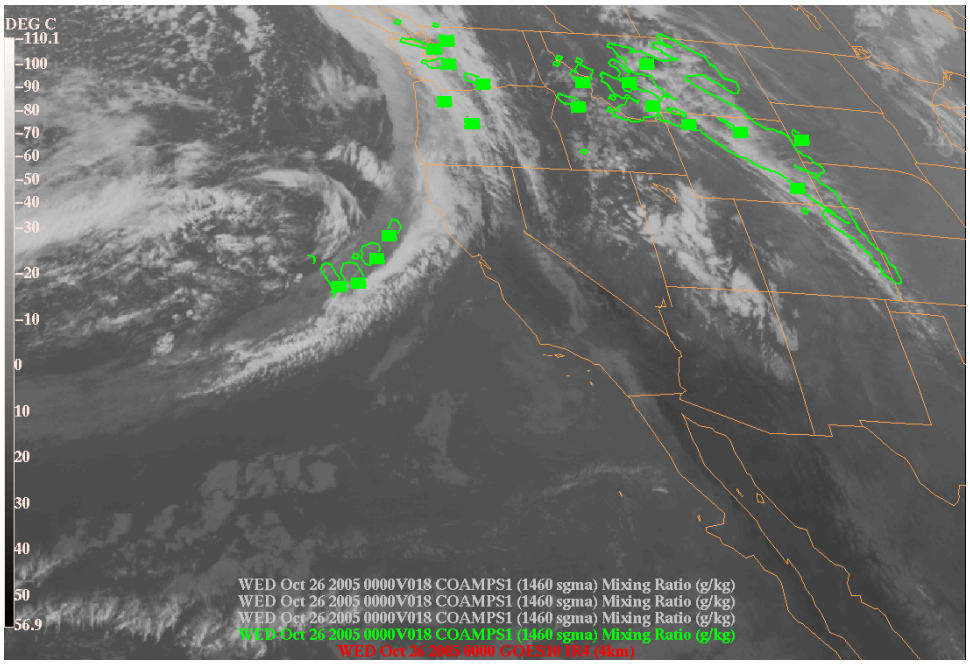

Figure 5.5.a. 1460 sigma ice water mixing ratio contours and corresponding IR image valid at 26/00Z. Labels have been omitted from the ice water mixing ratio contours.

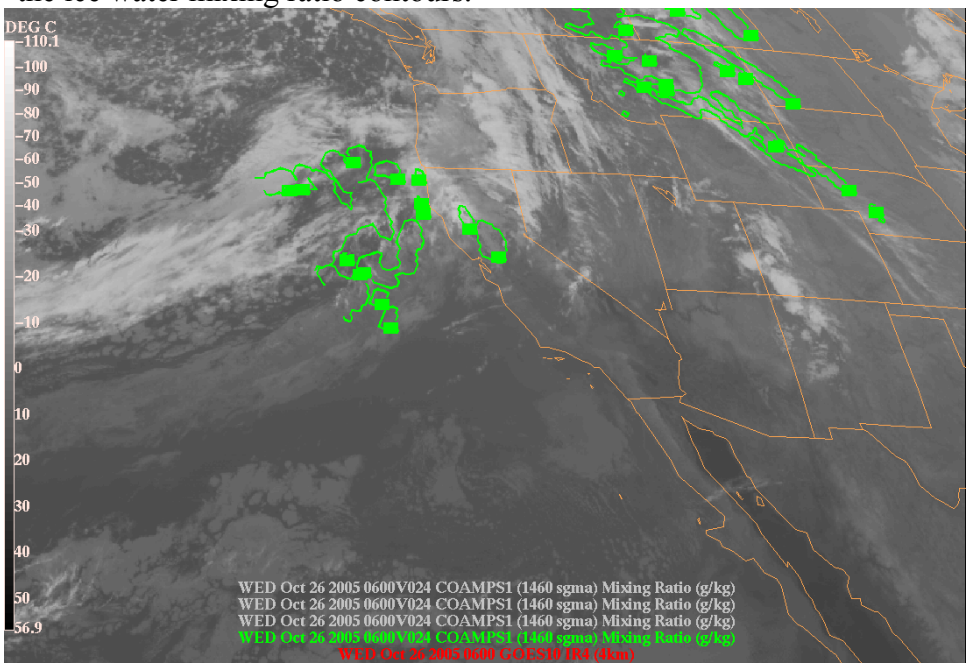

Figure 5.5.b. 1460 sigma ice water mixing ratio contours and corresponding IR image valid at 26/06Z. Labels have been omitted from the ice water mixing ratio contours.

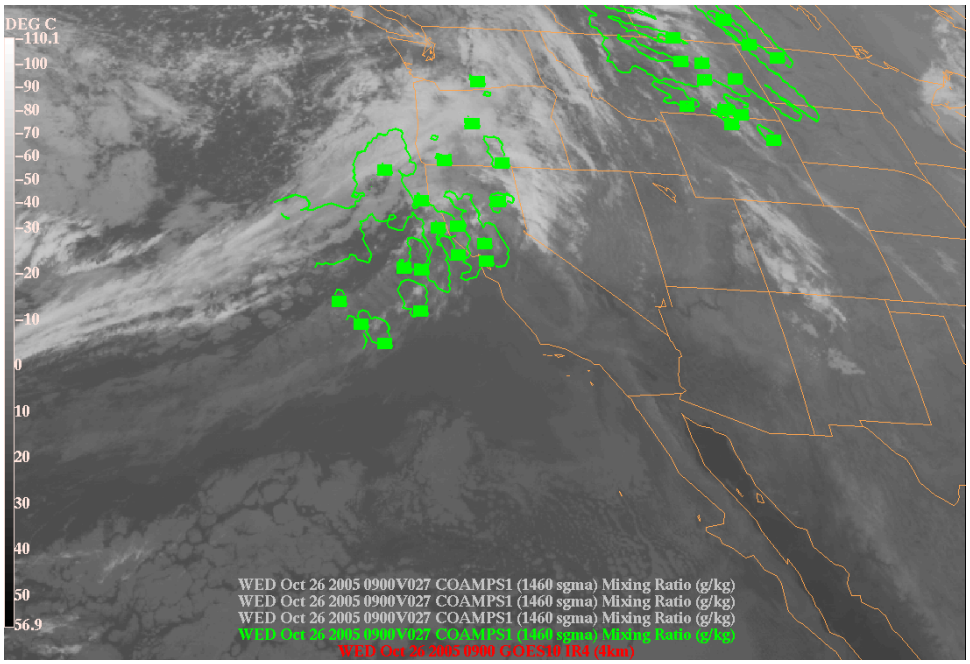

Figure 5.5.c. 1460 sigma ice water mixing ratio contours and corresponding IR image valid at 26/09Z. Labels have been omitted from the ice water mixing ratio contours.

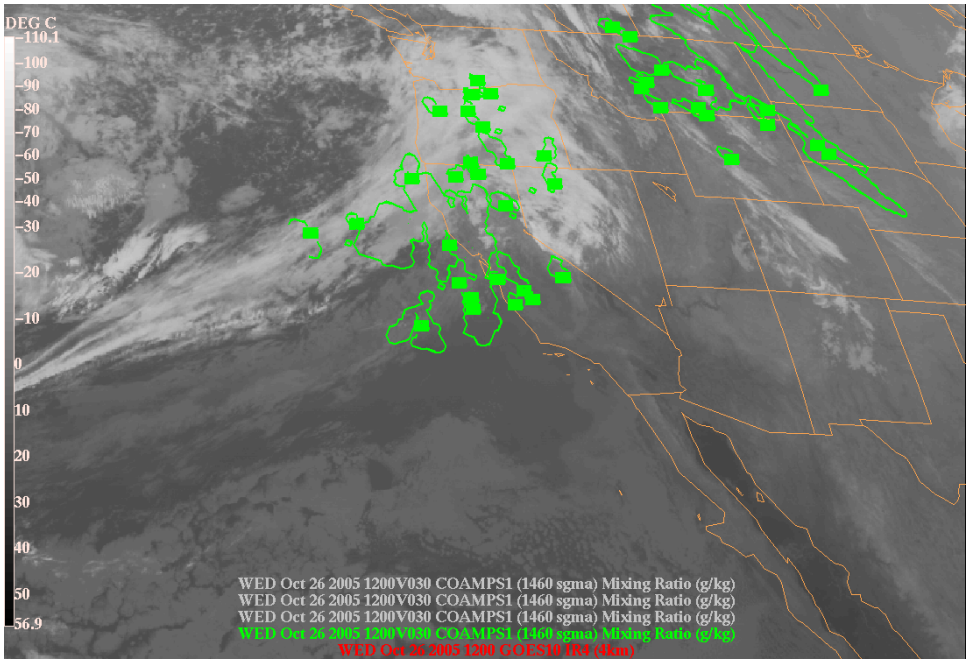

Figure 5.5.d. 1460 sigma ice water mixing ratio contours and corresponding IR image valid at 26/12Z. Labels have been omitted from the ice water mixing ratio contours.

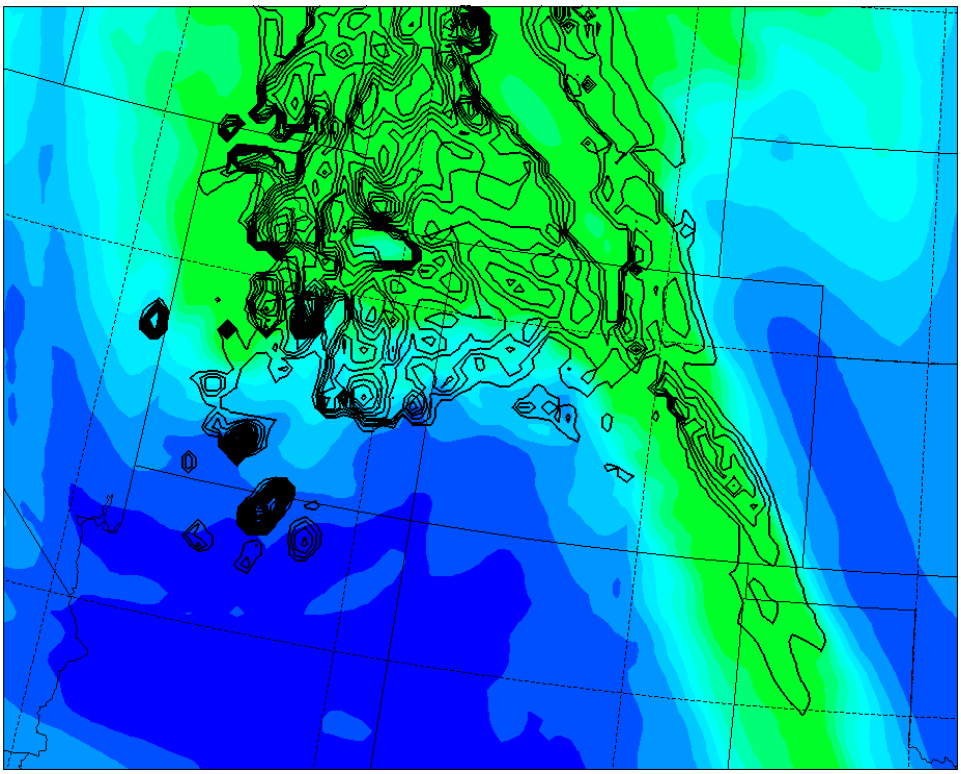

Figure 5.6.a. Relative humidity (with respect to ice) vs composite ice water mixing ratio for 26/00Z. Green shades indicate relative humidity of 90% and greater.

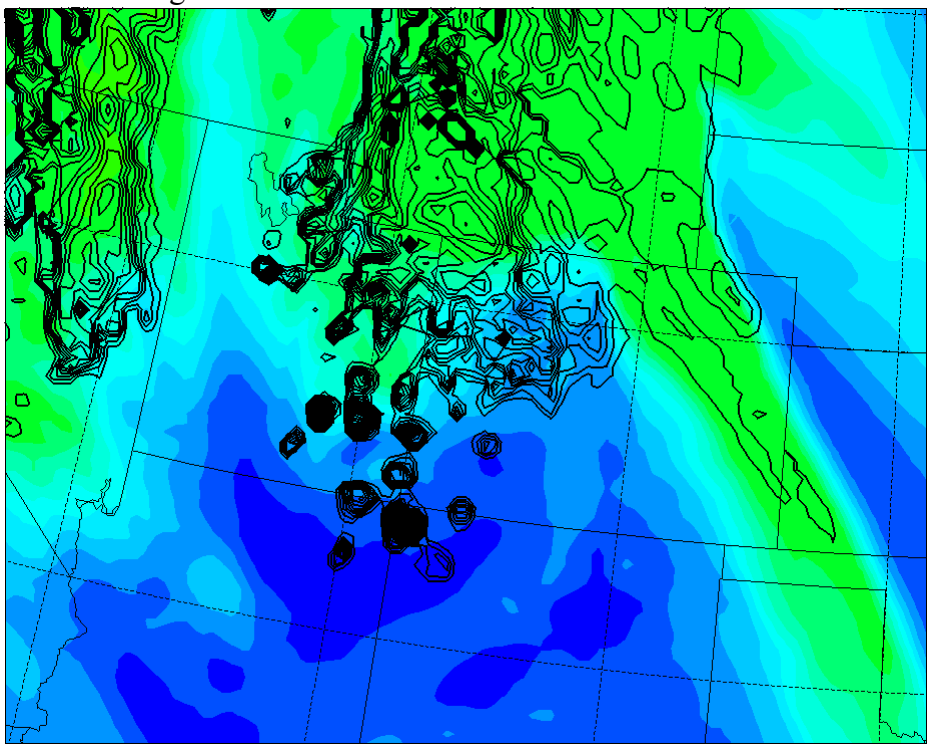

Figure 5.6.b. Relative humidity (with respect to ice) vs composite ice water mixing ratio for 26/06Z. Green shades indicate relative humidity of 90% and greater.

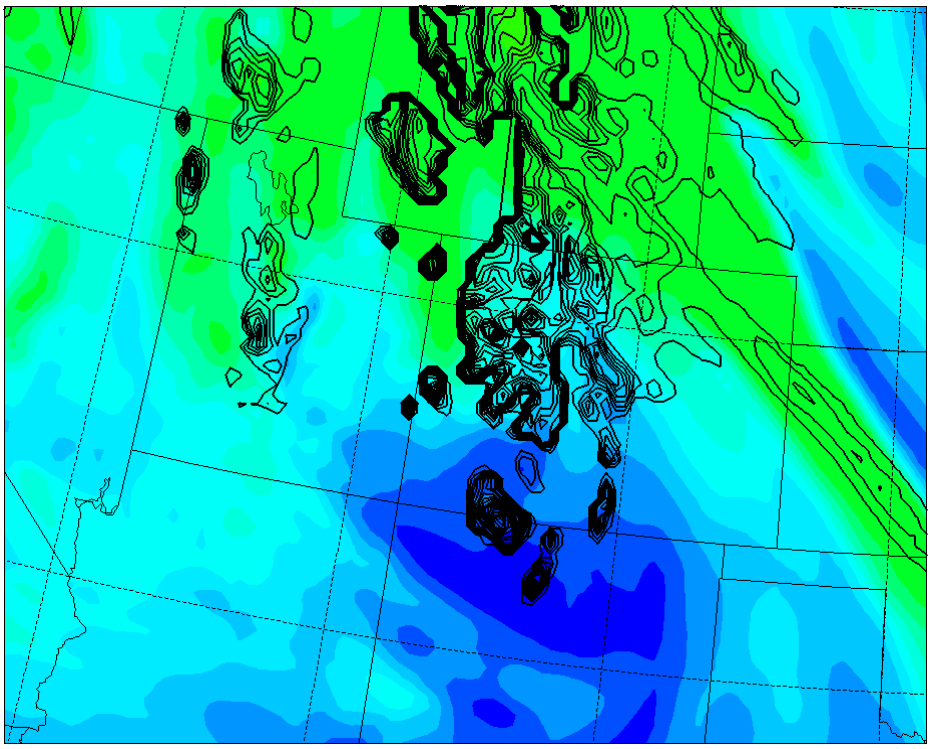

Figure 5.6.c. Relative humidity (with respect to ice) vs composite ice water mixing ratio for 26/12Z. Green shades indicate relative humidity of 90% and greater.

THIS PAGE INTENTIONALLY LEFT BLANK

VI. DISCUSSION

Case I involved a fairly well-organized upper-level low moving into the southwestern United States, with an initial moisture tap provided by tropical convective activity. The case was chosen to study the development/evolution of the cloud ice water field in a region of broad upward vertical motion. Although tropical convection was initially responsible for injecting moisture into the upper levels, the sustainment and development of ice water later in the period was due to this large-scale upward motion ahead of the upper-level low off the coast.

Case II focused on the model's handling of cirrus associated with an upper-level ridge downstream of an upper trof. Cirrus were present in two distinct locations: downstream of the ridge axis (in a typically non-generative area) and downstream of the upper trof to the west of the ridge. The cirrus near the low was much lower in altitude than the cirrus downstream of the ridge axis.

Both cases are very similar with regard to basic features, but evolution of the cirrus field in each case differs significantly due to ridge amplitude and available moisture at the source. The first case showed weaker ridge amplitude, but had a very strong initial moisture supply from below due to strong dynamic lifting associated with convection over the tropics. The second case had a very sharp ridge but the moisture source was not quite as strong as for the first case.

Despite these differences, the dynamics associated with the two cases are similar in some respects. In the first case, tropical convective activity initially injected large amounts of moisture into the upper atmosphere. That moisture was carried by upper-level winds in advance of a closed low into an area of widespread difluence ahead of the low. This acted to provide additional large-scale upward vertical motion of sufficient strength to promote widespread nucleation before confluence downstream suppressed cirrus formation. In the second case, lift associated with the upper trof resulted in cirrus formation, and the cirrus clouds were subsequently advected across the ridge axis and downstream by upper-level winds before dissipating in the downstream portion of the

ridge. In the second case, the model's tendency to link upward motions to ice production became apparent. Further study will help to determine if this is more generally the case.

VII. CONCLUSIONS AND RECOMMENDATIONS

The results show that vertical motions in the AFWA MM5 model appear strongly tied to presence of ice cloud, and that the ice forecast will live or die by correct forecasting of vertical motions together with moisture. As we noted in the first case, cirrus over the California/Arizona border in the satellite image shown in Figure 4.1.a were not forecast by the model (as shown in Figure 4.3.a). Figure 4.7.a does show relative humidity levels very slightly in excess of 90% over the location, so we can draw the conclusion that either lift was insufficient to produce ice or some microphysical aspect of the parameterization prevented cirrus formation. Indeed, vertical velocities diminished over the area through the case study period. In the second case, areas of cirrus were overforecast over parts of Colorado, Wyoming, Utah, and Idaho due to the forecast presence of upward motion and moisture in those areas. With the case studies presented in this thesis, it appears as though the 90 percent relative humidity field (with respect to ice) may be very useful as a first guess for anticipated cirrus coverage assuming the model is accurately handling timing and orientation of weather systems.

This study has examined AFWA MM5 strengths and weaknesses in forecasting cirrus development and evolution between the 18-30 hour forecast periods for two unique cases of interest. As we have seen, fully explaining development and evolution of cirrus based on dynamic factors alone is not possible, as there are only a limited number of dynamic factors involved in cirrus production that can be readily analyzed. Most factors involved in cirrus production take place on a scale smaller than we can analyze using standard analysis tools such as those used in preparation of this thesis. For a better understanding of potential weaknesses and strengths in cirrus forecasting with the MM5, it is necessary to analyze many different cases and compile results for comparison.

Perhaps the most thorough method for studying modeled production of cirrus would provide a researcher the ability to see the results of each term in the Reisner parameterization as the model ran over time, so each member's contribution to ice water production could be noted. This process would be performed at each model gridpoint in the domain, and then the applicable dynamics would be brought into consideration along

with the results of the Reisner scheme. The process would require automation due to the shear volume of data involved. Once these results were generated, the cloud mask results could be overlaid with an ice water composite in a similar manner to what was done in this thesis, and statistics could be generated to determine errors in coverage at each gridpoint on the model domain. Errors could then be studied and categorized according to their cause, whether related to the model's movement of features, errors in model dynamics, or insufficiencies in the parameterization.

The results of this study are valid for only two cases and therefore make it difficult to comment on the statistical accuracy of the MM5 when predicting cirrus over a variety of synoptic situations. Yet, it can be said that for the two cases analyzed there appears to be a link between upward motions in the model, moisture in the model (specifically, relative humidity with respect to ice in excess of 90%), and the presence of model-forecast ice cloud. Additional study at a deeper level is necessary to gain an understanding of the effects of microphysical details on AFWA MM5 ice cloud forecasts.

LIST OF REFERENCES

AFRL-VS-TR-2001-1549, Development and Validation of Improved Techniques for Cloud Property Retrieval from Environmental Satellites, Gary Gustafson and Robert P. d'Entremont, pp. 3-18, 17 November 2000.

Fletcher, N.H., 1962: *The Physics of Rain Clouds.* Cambridge University Press, UK.

Houze, Robert A., Jr., 1993: *Cloud Dynamics*, p.174, Academic Press, 573 pp.

Norquist, Donald C., and Robert P. d'Entremont, 2003: Analysis and Prediction of Cirrus-Top Altitude and Ice Water Path in a Mesoscale Area. Journal of Applied Meteorology: Vol. 42, No. 8, pp. 1092-1106.

Ou, Szu-Cheng, et. al., 2002: Laser Transmission-Backscattering through Inhomogeneous Cirrus Clouds. Applied Optics: Vol. 41, No. 27, pp. 5744-5754.

Reisner, J., R.M. Rasmussen, and R.T. Bruintjes, 1998: Explicit Forecasting of Supercooled Liquid Water in Winter Storms Using the MM5 Mesoscale Model. Quarterly Journal of the Royal Meteorological Society: Vol. 124B, pp. 1071-1107.

Schmidt, Jerome. Re: MM5 Ice Water Representation. E-mail from jerome.schmidt@nrlmry.navy.mil, 14 February 2006.

Starr, David O'C., and Donald P. Wylie. 1990: The 27-28 October 1986 FIRE Cirrus Case Study: Meteorology and Clouds. Monthly Weather Review: Vol. 118, No. 11, pp. 2259-2287.

Starr, David O'C., and Andrew R. Lare. 1993: Meteorological Analysis of the December 4-6 FIRE Cirrus-II case. *FIRE Cirrus Science Results 1993*, (Breckenridge, CO), NASA Conf. Publ. 3238, pp. 92-97.

Starr, David O'C., and Andrew R. Lare. 1993: Meteorological Analysis of the November 25 FIRE Cirrus-II case: A well-defined ridge-crest cirrus system over Oklahoma. *FIRE Cirrus Science Results 1993*, (Breckenridge, CO), NASA Conf. Publ. 3238, pp.144-147.

THIS PAGE INTENTIONALLY LEFT BLANK

INITIAL DISTRIBUTION LIST

1. Defense Technical Information Center
   Ft. Belvoir, Virginia

2. Dudley Knox Library
   Naval Postgraduate School
   Monterey, California